S. Culina, A.I. Lalanne et al., Islet-reactive $CD8^+$ T-cell frequencies in the pancreas but not blood distinguish type 1 diabetes from healthy donors.

Supplementary Materials

Materials and Methods.

Fig. S1. Cytokine secretion and cytotoxicity of $ZnT8_{186-194}$-reactive $CD8^+$ T cells from T1D patient D222D.
Fig. S2. $CD8^+$ T-cell recognition and HLA-A2 binding of $ZnT8_{186-194}$ and $ZnT8_{185-194}$ epitope variants.
Fig. S3. Ag sensitivity correlates with Ag avidity and polyfunctionality in $ZnT8_{186-194}$-reactive $CD8^+$ T-cell clones.
Fig. S4. Modulation of HLA Class I and ZnT8 expression in human β-cell lines.
Fig. S5. TCR sequences of $ZnT8_{186-194}$-reactive $CD8^+$ T-cell clones.
Fig. S6. $ZnT8_{186-194}$-reactive clonotype-specific TaqMan assays.
Fig. S7. Gating strategy for the analysis of $ZnT8_{186-194}$, $MelanA_{26-35}$ and Flu MP_{58-66} MMr^+CD8^+ T cells.
Fig. S8. IFN-γ secretion by $ZnT8_{186-194}$-reactive $CD8^+$ T cells.
Fig. S9. Gene expression in *ex-vivo* single-sorted $ZnT8_{186-194}$ MMr^+CD8^+ T cells.
Fig. S10. Extended combinatorial MMr panel for the analysis of multiple islet-reactive $CD8^+$ T-cell populations, and reproducibility of *ex-vivo* MMr assays.
Fig. S11. CD27, CD28 and CD95 expression on $ZnT8_{186-194}$-reactive $CD8^+$ T cells.
Fig. S12. Representative MMr and CD45RA/CCR7 dot plots for HLA-$A2^+$ and HLA-$A2^-$ healthy donors depicted in Fig. 6F-G.
Fig. S13. Correlation between the frequency of MMr^+CD8^+ T cells and the Ag-experienced fraction within the same MMr^+CD8^+ population.
Table S1. Summary of $ZnT8_{186-194}$-reactive $CD8^+$ T-cell clones.
Table S2. Characteristics of study subjects for *in-silico TRB* analyses.
Table S3. Characteristics of HLA-$A2^+$ study subjects for *ex-vivo* MMr studies.
Table S4. Characteristics of HLA-$A2^+$ and HLA-$A2^-$ healthy donors for *ex-vivo* MMr studies.
Table S5. Characteristics of nPOD cases for *in-situ* $ZnT8_{186-194}$ MMr staining.
Table S6. Primers used for gene expression analysis of the individual $ZnT8_{186-194}$ MMr^+CD8^+ T cells depicted in Fig. S9A.

Members of the ImMaDiab Study Group.

Excel file. Raw data from figure graphs.

Materials and Methods

Study design. The objective of this study was to identify the features of islet-reactive $CD8^+$ T cells that associate with T1D. Hypotheses were formulated on a prospective basis guided by the data. Based on a detailed analysis of $ZnT8_{186-194}$-reactive $CD8^+$ T-cell clones (listed in Table S1), we initially hypothesized that peripheral autoreactivity occurs independently of disease status. This hypothesis was substantiated using HLA-A2 MMrs to quantify and characterize islet-reactive $CD8^+$ T cells directly *ex-vivo* (donors listed in Table S3). Next, we hypothesized that this widespread autoimmune repertoire stems from a universal leakiness of central tolerance, which was verified by thymic gene expression studies and by comparing HLA-A2-restricted Ag-reactive $CD8^+$ T-cell population frequencies in HLA-$A2^+$ vs. HLA-$A2^-$ donors (listed in Table S4). Finally, we hypothesized that the lack of distinguishing features in the periphery reflects sequestration of the disease-relevant subset in the pancreas. This hypothesis was confirmed by *in-situ* MMr staining of pancreatic sections (donors listed in Table S5). Following power analysis, age/sex-matched, unblinded case-control sets were selected from donors recruited at affiliated Diabetology Units. Samples were processed in batch, and no outliers were excluded. All *in-vitro* experiments were performed on at least two separate occasions. For *ex-vivo* MMr analyses, undersampled data-points were excluded, as detailed in Fig. 5-6.

Study approval. All subjects provided written informed consent. Ethical approval was granted by the Comité de Protection des Personnes Ile de France 1-2 (AOR10049, K091101, A01094-53) and by the Institutional Review Boards of the Cambridge Royal Free Hospital (08/H0720/25), the Benaroya Research Institute (7109-147), the University of Heidelberg (367/2002) and the University of Florida Health Center (nPOD Project). The ImMaDiab study is registered at www.clinicaltrials.gov (NCT01747967).

Peptides, MMrs and HLA-A2 binding measurements. Peptides $ZnT8_{186-194}$ (VAANIVLTV) and its *B. stercoris* WP_060386636.1 mimotope (KAANIVLTV), $ZnT8_{185-194}$ (AVAANIVLTV), $MelanA_{26-35}$ (A27L variant; ELAGIGILTV), Flu MP_{58-66} (GILGFVFTL), PPI_{6-14} (RLLPLLALL), PPI_{15-24} (ALWGPDPAAA), $GAD_{114-122}$ (VMNILLQYV), IA-$2_{805-813}$ (VIVMLTPLV), $IGRP_{265-273}$ (VLFGLGFAI), EboV $NP_{202-210}$ (RLMRTNFLI) and HCV $PP_{1406-1415}$ (KLVALGINAV) were synthesized at >85% purity (ChinaPeptides). Peptide-HLA-A2 affinity and stability assays were performed as detailed in Fig. S2. HLA-A2 MMrs were produced as described (*39*), and staining was performed in the presence of 50 nM dasatinib (*11*). For Fig. 2B, MMr MFIs were normalized to that of D222D clone 2 in the presence of dasatinib.

Cloning of $ZnT8_{186-194}$-reactive $CD8^+$ T cells. Frozen-thawed PBMCs (2-10x10^6) were stained with dual fluorochrome-labeled $ZnT8_{186-194}$ MMrs, either directly *ex-vivo* or after 10 days of acDC culture (*8*) in the absence or presence of 1 µM peptide ($ZnT8_{186-194}$ or $ZnT8_{185-194}$). Double-positive events were then sorted as single cells into individual wells of a U-bottom 96-well plate. Each sort well contained 200,000 irradiated PBMCs, 5% Cellkines (Zeptometrix), 200 IU/ml Proleukin, 25 ng/ml IL-15, 1 µg/ml phytohemagglutinin (PHA)-L (Sigma), penicillin/streptomycin and amphotericin B. Medium was replenished every 3 days

without PHA-L. Expanding clones were selected by visual inspection, transferred into 48-well plates for specificity testing and restimulated as above every 2-3 weeks.

Antigen recall assays. Peptide-pulsed HLA-A2$^+$ LCLs or K562 cells transduced with HLA-A2, CD80 and 4-1BBL (a kind gift from Dr. J. Riley, University of Pennsylvania, Philadelphia, PA) were labeled with CellTrace Violet (Life Technologies) and incubated with T cells at an E/T ratio of 2/1 for 6 h in the presence of 10 μg/ml brefeldin A. Intracellular cytokine staining was performed using BD Cytofix/Cytoperm reagents and analyzed using a BD LSR Fortessa cytometer. CD107a staining was performed with a FITC-labeled mAb (clone H4A3, BD). Polyfunctionality indices were calculated as described (*12*).

Cytotoxicity assays. LCL, K562-A2 or K562-A2/ZnT8 target cells were labeled with CellTrace FarRed (Life Technologies), dispensed into 96-well flat-bottom plates at 10^5 cells/well and co-cultured with different numbers of CFSE-labeled T cells for 6-24 h. After staining with Live/Dead Aqua (Life Technologies) and fixation, a set number of CompBeads (BD) was added to each well. Flow cytometric analysis was performed by counting the numbers of CFSE$^-$FarRed$^+$Live/Dead$^-$ targets for each condition, normalized to equal numbers of CompBeads. Percent lysis was calculated as 100 × (live targets cultured alone) – (live targets in the presence of T cells) / (live targets cultured alone). Blocking experiments were conducted with concanamycin A (100 nM; Sigma), brefeldin A (5 μg/ml; Sigma) and the anti-FasL antibody NOK-1 (5 μg/ml; BD).
The EndoC-βH2 cell line (HLA-A*01/03, -B*07/08, -C*07/07) was described previously (*40*), and the ECN90 cell line (HLA-A*02:01/03, -B*40/49, -C*03/07) was derived from a human neonatal pancreas using similar protocols. Real-time cytotoxicity assays on β-cell lines were performed using the xCELLigence system (ACEA Biosciences). Briefly, β cells were dispensed into 96-well E-plates and pretreated as indicated. After resting for 20 h and pulsing with 10 μM peptide or DMSO for 2 h, T cells were added at an E/T ratio of 2/1, and impedance was recorded every 5-15 min for 4 h. Cell indices were normalized to values at the time of T-cell addition (t=0) and transformed to percent lysis.

TCR sequencing, in-silico analyses and clonotype-specific TaqMan assays. TRA and *TRB* gene expression was analyzed using a template-switch anchored RT-PCR (*41*) for T-cell clones and a multiplex nested PCR (*42*) for single-sorted cells. Gene usage was determined according to the ImMunoGeneTics (IMGT) nomenclature.
The *TRB* database (Adaptive Biotechnologies) used for *in-silico* analyses was derived from the donors listed in Table S2. TaqMan assays (Life Technologies; Fig. S6) were applied to cDNA samples from naïve (CD45RA$^+$CCR7$^+$) and Ag-experienced (CD45RA$^+$CCR7$^-$ or CD45RA$^-$CCR7$^{+/-}$) CD4$^+$ and CD8$^+$ T cells bulk-sorted from age/sex-matched cohorts incorporating 83 T1D patients [age 34 years (17-59), 51% females, T1D duration 8 years (0.1-55), 51% HLA-A2$^+$] and 93 healthy donors [age 34 years (17-60), 47% females, 41% HLA-A2$^+$]. cDNA samples were amplified using clonotype-specific TaqMan primers for 18 cycles, followed by real-time qPCR using clonotype-specific TaqMan assays on Fluidigm 96.96 microfluidic chips with a BioMark HD qPCR system. Amplification curves for

individual assays were examined and compared with curves from a *TRB* constant region assay as a control for *TRB* templates in each reaction.

Ex-vivo analysis of ZnT8$_{186-194}$-reactive CD8$^+$ T cells. Cryopreserved PBMCs from T1D and healthy donors (Table S3) were magnetically depleted of CD8$^-$ cells (StemCell Technologies), stained with the combinatorial MMr panels (*9*) detailed in Fig. S7 and S10 and acquired using a BD FACSAria III cytometer. IFN-γ ELISpot assays were performed as described (*7*). Single-cell gene expression analysis is detailed in Fig. S9A and Table S6.

Gene expression in human mTECs. Human thymus samples were obtained from children undergoing corrective cardiac surgery at the University of Heidelberg, Germany. mTECs were purified as described (*13*). Sorted total, immature and mature mTECs (CD45$^-$ EpCAM$^+$CDR2$^-$) were independently validated for gene expression of the tissue-restricted Ags β-casein and MelanA (*13*). Amplified bands were sequences to confirm identity with the expected *SLC30A8* and *INS* regions. *SLC30A8* exons were annotated with reference to Ensembl ID ENST00000427715. The *INS* PCR covered all *INS* transcripts except ENST00000512523 (product 1) and ENST00000421783 (product 2).

In-situ ZnT8$_{186-194}$ MMr staining. *In-situ* staining was performed as described (*2*). Briefly, unfixed, frozen sections were dried for 2 h, loaded with 1 µg of MMrs overnight at 4°C, washed gently with phosphate-buffered saline and fixed in 2% paraformaldehyde for 10 min. After a further wash, endogenous peroxidase activity was blocked with 0.3% H_2O_2. Sections were then incubated serially with rabbit anti-phycoerythrin, horseradish peroxidase-conjugated swine anti-rabbit and 3,3'-diaminobenzidine tetrahydrochloride substrate (Thermo Scientific). After a final wash, sections were counterstained with hematoxylin, dehydrated *via* sequential passages in 95-100% ethanol and xylene, mounted and analyzed using a Nikon Eclipse Ni microscope with NIS-Elements Analysis D software v4.40.

Statistical analysis. Data are shown as median (range) or mean±SEM. Significance was assessed using two-tailed tests with a cut-off value of α=0.05, as detailed for each figure.

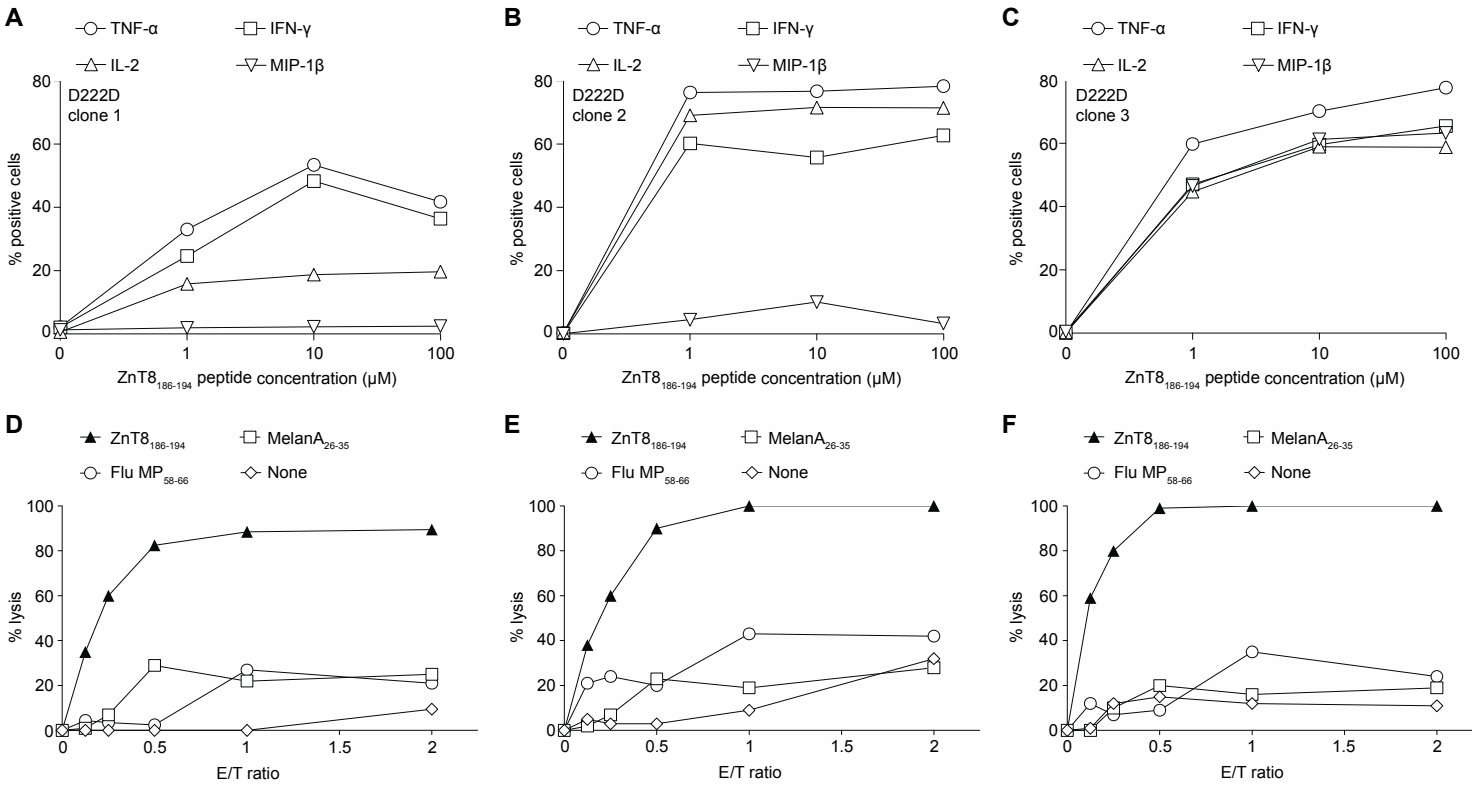

Fig. S1. Cytokine secretion and cytotoxicity of ZnT8$_{186-194}$-reactive CD8$^+$ T cells from T1D patient D222D. (**A-C**) D222D clone 1 (A), 2 (B) or 3 (C) were stimulated for 6 h with K562-A2 cells pulsed with the indicated peptide concentrations. Graphs display percent intracellular cytokine$^+$ cells calculated after gating on viable CD8$^+$ cells, as shown in Fig. 1C. The following antibodies were used: anti-TNF-α-APC (clone MAb11, BD), anti-IFN-γ-PE (clone 4S.B3, eBioscience), anti-IL-2-PE/Cy7 (clone MQ1-17H12, eBioscience) and anti-MIP-1β-FITC (clone 24006, R&D). (**D-F**) FarRed-labeled HLA-A2$^+$ LCL target cells were pulsed with the indicated peptides and cultured with CFSE-labeled D222D clones 1 (D), 2 (E) or 3 (F) at increasing E/T ratios. Live FarRed$^+$ target cells were counted at 24 h and normalized to a fixed number of beads added to each well. Percent lysis is plotted for each graph, calculated as 100 × (live targets cultured alone) – (live targets in the presence of T cells) / (live targets cultured alone). Results are representative of three independent experiments. For panels A-C, results are shown from a separate experiment than depicted in Fig. 1C. For panels D-F, results are shown from the three separate clones, with raw data for D222D clone 3 depicted in Fig. 1D, and pooled data for all three clones depicted in Fig. 1E.

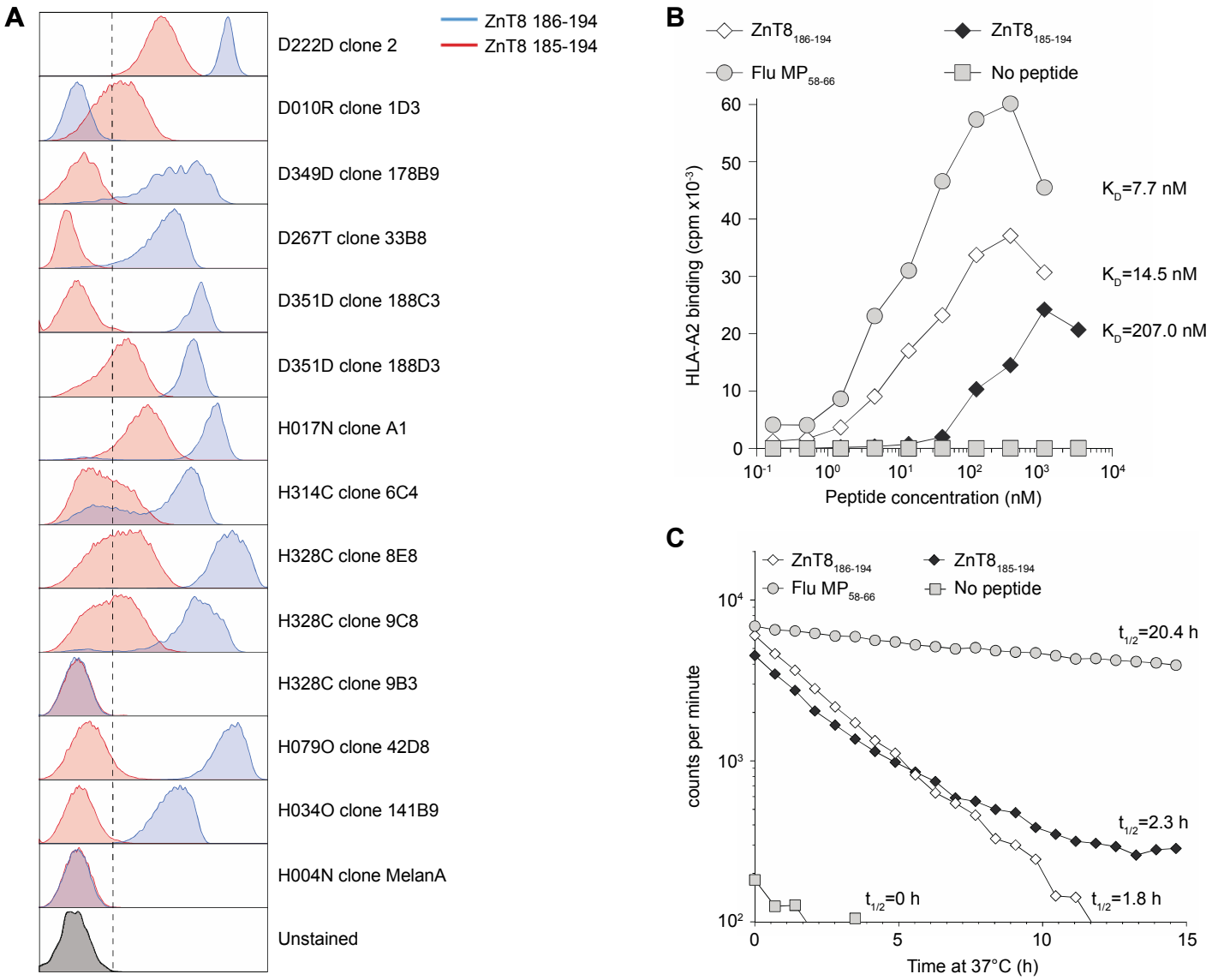

Fig. S2. CD8$^+$ T-cell recognition and HLA-A2 binding of ZnT8$_{186\text{-}194}$ and ZnT8$_{185\text{-}194}$ epitope variants. (**A**) The indicated clones were stained with HLA-A2 MMrs loaded with either ZnT8$_{186\text{-}194}$ (VAANIVLTV; blue profiles) or ZnT8$_{185\text{-}194}$ (AVAANIVLTV; red profiles) in the presence of dasatinib. MMr fluorescence intensities registered in separate runs were made comparable by using the same flow cytometer settings, by recalibrating the cytometer for each run using Spherotech Rainbow Calibration particles, and by including a reference D222D clone (thawed cryovials from the same freeze) in all experiments. The MMr fluorescence registered in each run for the reference D222D clone was also used to further normalize the median fluorescence intensities plotted in Fig. 2B. (**B**) *In-vitro* HLA-A2 binding affinity measurements for the ZnT8$_{186\text{-}194}$ (white diamonds) and ZnT8$_{185\text{-}194}$ peptides (black diamonds). Recombinant HLA-A2 (0.7 nM) was mixed in 96-well polypropylene plates (Nunc) with β_2-microglobulin (β_2M; 25-50 nM) and the indicated peptide (5-fold titrations) in phosphate-buffered saline supplemented with 0.1% Lutrol F-68 and allowed to form complexes at 18°C for 48 h. Amounts of each peptide-HLA complex were determined using an AlphaScreen assay (Perkin Elmer) with streptavidin-conjugated donor beads and W6/32 anti-HLA Class I antibody-conjugated acceptor beads. Peptide-HLA complexes (10 µl) were transferred to 384-well OptiPlates (Perkin Elmer) in duplicates, mixed with 30 µl each of streptavidin-conjugated donor beads and W6/32-conjugated acceptor beads, and

incubated in the dark for 6-8 h at room temperature. Plates were analyzed using an Envision reader (Perkin Elmer). (**C**) *In-vitro* HLA-A2 stabilization assays with the $ZnT8_{186-194}$ and $ZnT8_{185-194}$ peptides. Recombinant HLA-A2 molecules were incubated with the indicated peptides and the corresponding dissociation rates were monitored over time. Briefly, biotinylated recombinant HLA-A2 (30 nM) was mixed with peptide (10 mM) and ^{125}I-labeled β_2M (25,000 cpm/well), transferred to a 96-well FlashPlatePlus (Perkin Elmer), and allowed to form complexes overnight at 18°C. Dissociation was initiated by adding unlabeled β_2M at a final concentration of 360 nM and monitored by consecutively reading the microplates in a TopCount NXT scintillation counter (Perkin Elmer) at 37°C for 15 h. K_D affinity (B) and half-life ($t_{1/2}$) values (C) are displayed, as calculated using a non-linear regression fit (GraphPad Prism 5). Results are representative of three independent experiments.

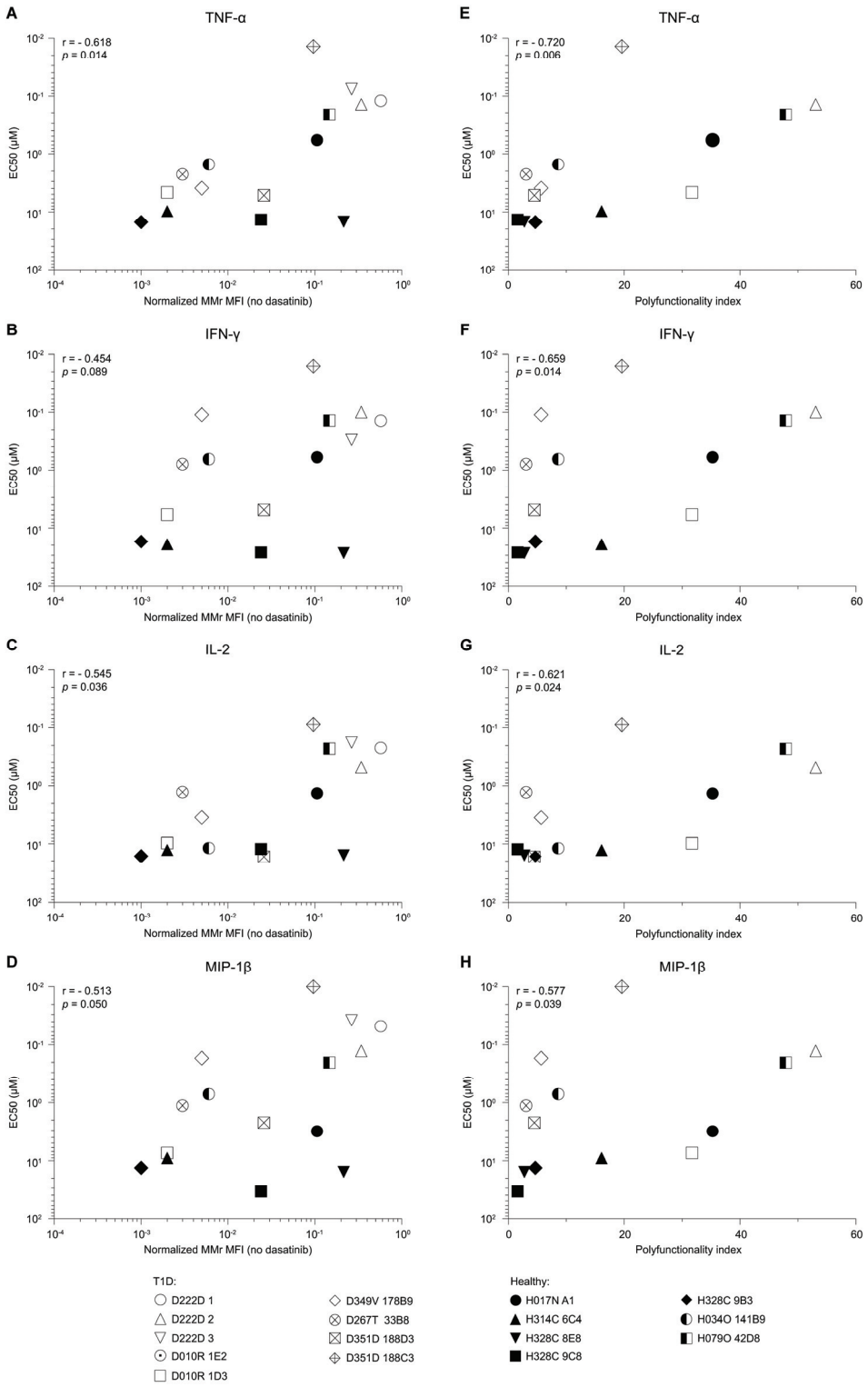

Fig. S3. Ag sensitivity correlates with Ag avidity and polyfunctionality in ZnT8$_{186-194}$-reactive CD8$^+$ T-cell clones. (**A-D**) The indicated CD8$^+$ T-cell clones generated from T1D and healthy subjects (white and black symbols, respectively, as in Fig. 2) were compared for normalized MMr MFI in the absence of dasatinib (from Fig. 2B; x-axis) *vs.* ZnT8$_{186-194}$ peptide EC50 for the indicated cytokine responses (from Fig. 2D; y-axis). EC50 values are plotted from higher to lower, corresponding to increasing Ag sensitivity. (**E-H**) The same clones were compared for polyfunctionality index (from Fig. 2F; x-axis) *vs.* ZnT8$_{186-194}$ peptide EC50 (as in panels A-D). The corresponding Spearman r and *p* values are displayed for each panel.

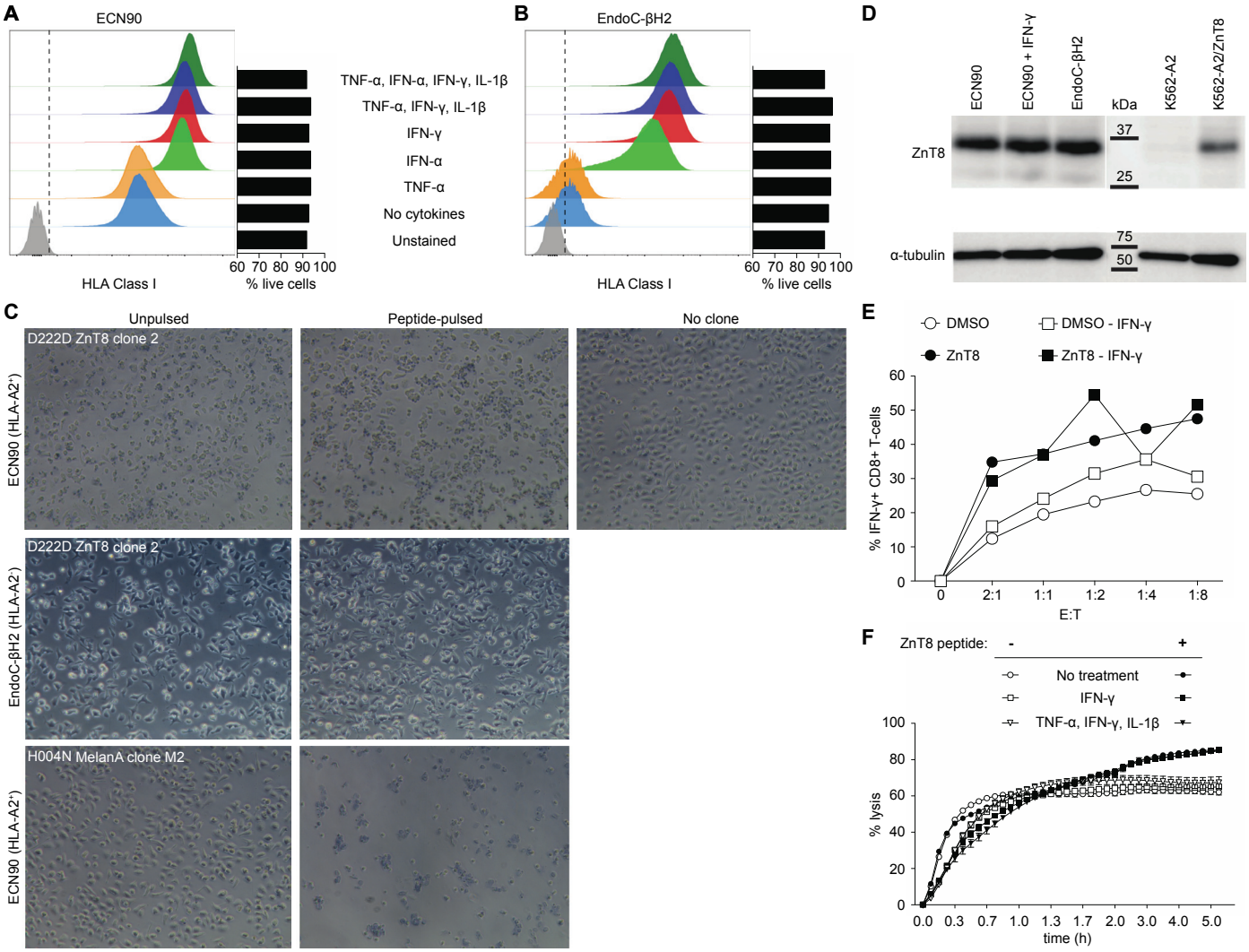

Fig. S4. Modulation of HLA Class I and ZnT8 expression in human β-cell lines. (**A-B**) Surface HLA Class I expression (anti-HLA-A, B, C antibody W6/32, labeled in-house with AlexaFluor647) and Live/Dead Red viability of HLA-A2$^+$ ECN90 (A) and HLA-A2$^-$ EndoC-βH2 cell lines (B) with and without exposure to the indicated cytokines for 18 h. The following cytokine cocktails were used: TNF-α alone (1,100 U/ml); IFN-α alone (500 U/ml); IFN-γ alone (500 U/ml); TNF-α, IFN-γ and IL-1β (1,100 U/ml, 2,000 U/ml and 1,000 U/ml, respectively); TNF-α, IFN-α, IFN-γ and IL-1β (2,500 U/ml, 1,000 U/ml, 500 U/ml and 50 U/ml, respectively). Results are representative of three independent experiments. (**C**) Representative optical microscopy images (10X magnification) of wells in which ZnT8$_{186-194}$-reactive D222D clones or MelanA$_{26-35}$-reactive clones were co-cultured with HLA-A2$^+$ ECN90 or HLA-A2$^-$ EndoC-βH2 cells for the cytotoxicity assays depicted in Fig. 3D-G. T cells were removed by gentle washing and the remaining cells were stained with Trypan Blue. Two independent experiments were performed. (**D**) ZnT8 expression in ECN90 and EndoC-βH2 β-cell lines pretreated with or without IFN-γ (500 U/ml, 18 h), as assessed by Western blot using an anti-ZnT8 antibody (clone 17H2.4, produced in-house). K562-A2 cells transduced or not with a full-length ZnT8 plasmid are shown as positive and negative controls, respectively. α-tubulin expression is shown as a loading control. (**E**) IFN-γ recall

assay for D222D clone 2 on ECN90 cells pretreated with or without IFN-γ (500 U/ml, 18 h), washed and pulsed with DMSO or 10 μM $ZnT8_{186-194}$ peptide for 2 h. A fixed number of T-cell effectors was co-cultured with increasing numbers of ECN90 targets for 6 h. Percent IFN-γ^+ cells was calculated from plots gated on viable $CD8^+$ cells. (**F**) Real-time cytotoxicity assays for D222D clone 2 in the presence of ECN90 cells (E/T ratio 2/1) pretreated with or without the indicated cytokines for 18 h. Results in panels D-F are representative of at least two independent experiments.

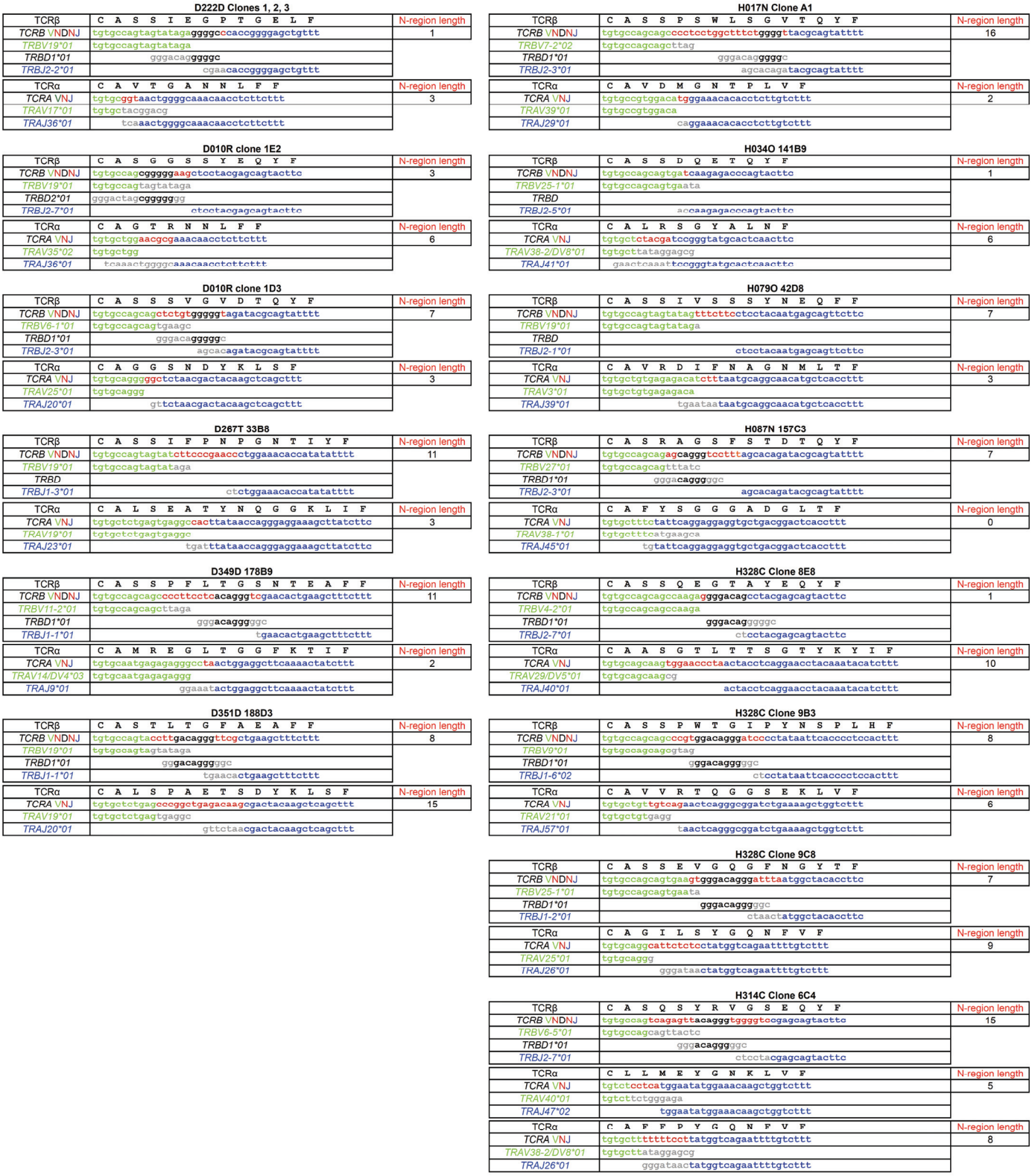

Fig. S5. TCR sequences of ZnT8$_{186\text{-}194}$-reactive CD8^{+} T-cell clones. Clones isolated from T1D patients are shown on the left and clones isolated from healthy donors are shown on the right. Nucleotide sequences rearranged from the indicated V (green), D (black) and J (blue) genes are shown for each clone. Nucleotide additions at the V-D, D-J and V-J junctions are shown in red and the corresponding N-region length is indicated (right column).

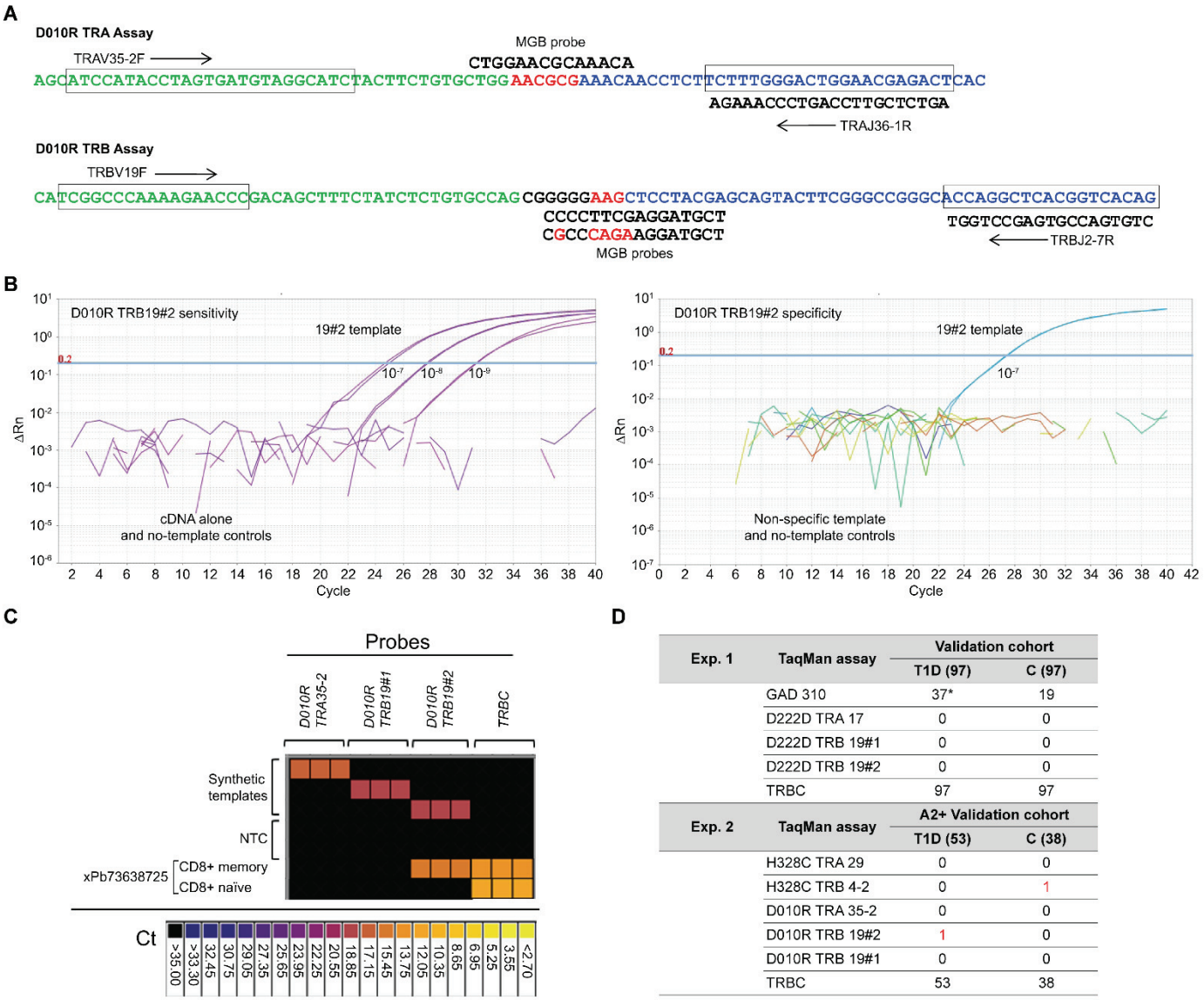

D

Exp. 1	TaqMan assay	Validation cohort	
		T1D (97)	C (97)
	GAD 310	37*	19
	D222D TRA 17	0	0
	D222D TRB 19#1	0	0
	D222D TRB 19#2	0	0
	TRBC	97	97
Exp. 2	**TaqMan assay**	**A2+ Validation cohort**	
		T1D (53)	**C (38)**
	H328C TRA 29	0	0
	H328C TRB 4-2	0	1
	D010R TRA 35-2	0	0
	D010R TRB 19#2	1	0
	D010R TRB 19#1	0	0
	TRBC	53	38

Fig. S6. ZnT8$_{186\text{-}194}$-reactive clonotype-specific TaqMan assays. (**A**) TaqMan assays were designed for the ZnT8$_{186\text{-}194}$-reactive CDR3 regions of the rearranged *TRA* (top) and *TRB* genes (bottom) from clones D010R 1E2, H328C 8E8 and D222D by placing forward primers in the V region and reverse primers in the J region of each transcript (black fonts). A 6-carboxyfluorescein (FAM)-labeled minor groove binder (MGB) probe was designed to cover the unique N(D)N region of each chain. For *TRBV19*$^+$ CDR3β regions (clones D010R and D222D), two unique nucleotide sequences were screened using two different probes (TRB19#1 and TRB19#2). Sequences corresponding to the V, D, N and J regions are shown in green, black, red and blue, respectively. The example shows TaqMan assays for the D010R clonotype. (**B**) Clonotype-specific TaqMan assays were validated using synthetic DNA templates (Life Technologies) for clonotype-specific or irrelevant *TRA* and *TRB* sequences. Ten-fold dilutions of the templates (from 10^{-7} to 10^{-9}; left panel, purple profiles) were spiked into naïve CD8$^+$ T-cell cDNA and amplified by qPCR. As shown for the D010R TRB19#2 probe, the sensitivity was 10^{-9}, equivalent to 100 copies of template (equivalent to ~1 T cell). The right panel shows that non-specific DNA templates and no-template controls (colored profiles) were not amplified. The blue line marks the detection threshold, set at a change in normalized reporter value (ΔRn) of 0.2. (**C**) Clonotype-specific TaqMan assays were used to screen cDNA from pooled naïve (CD45RA$^+$CCR7$^+$) or Ag-experienced (CD45RA$^+$CCR7$^-$ or

CD45RA$^-$CCR7$^{+/-}$) CD4$^+$ or CD8$^+$ T cells isolated from T1D or age/sex-matched healthy donors. Samples were pre-amplified with the pooled clonotype assays, and the products were used for real-time qPCR on a Fluidigm platform. Representative results are shown for the D010R *TRA* and *TRB* probes depicted in panels A-B, along with a *TRBC* probe included as a positive control for *TRB* templates in each sample. Results are shown for T1D patient xPb73638725 testing positive on memory and negative on naïve CD8$^+$ T cells. NTC, no-template controls. (**D**) Summary of the results obtained by screening T1D and control (C) healthy donors (number of subjects indicated in parentheses) with the D222D ZnT8 and control GAD clonotype-specific probes (experiment 1, top panel) and with the H328C and D010R clonotype-specific probes (experiment 2, bottom panel; only HLA-A2$^+$ subjects were analyzed). The number of subjects with ≥1 positive sample for each of the indicated assays is reported.

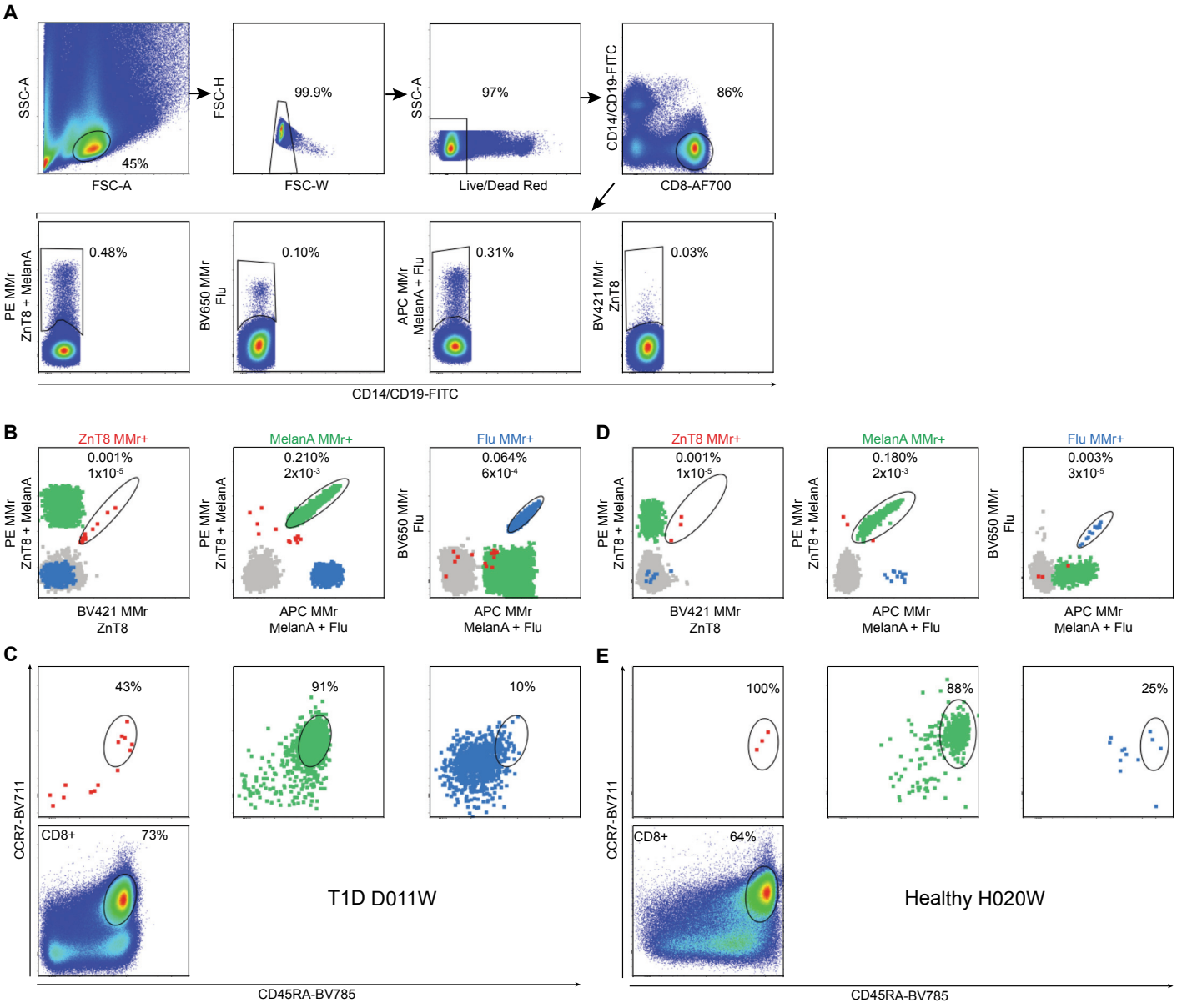

Fig. S7. Gating strategy for the analysis of ZnT8$_{186-194}$, MelanA$_{26-35}$ and Flu MP$_{58-66}$ MMr^{+}CD8^{+} T cells. (**A**) After magnetic depletion of CD8^{-} cells in frozen-thawed PBMCs from T1D patient #D011W, cells were sequentially gated on small lymphocytes, singlets, live cells (Live/Dead Red^{-}), CD8^{+} T cells (FITC-CD14/CD19^{-}, AlexaFluor700-CD8^{+}; clones 61D3, HIB19, RPA-T8, respectively; eBioscience) and total PE^{+}, BV650^{+}, APC^{+} and BV421^{+} MMr^{+} T cells. ZnT8$_{186-194}$ MMr-PE/BV421^{+}, MelanA$_{26-35}$ MMr-PE/APC^{+} and Flu MP$_{58-66}$ MMr-APC/BV650^{+} events were visualized using the gating strategy previously detailed for combinatorial MMr staining (*9*) and FlowJo v10 software (Tree Star). The staining panel also included anti-CD45RA-BV785 (clone HI100, BioLegend) and anti-CCR7-BV711 (clone 150503, BD). (**B**) The final readout obtained for T1D patient #D011W after gating out events positive for <2 or >2 MMr fluorochromes is shown, with events corresponding to each epitope-reactive population depicted in different colors within each plot, and MMr^{-} events depicted in grey. (**C**) Percent naïve (CD45RA^{+}CCR7^{+}) cells is shown after gating on the corresponding MMr^{+} fractions, with the distribution of total CD8^{+} T cells shown for comparison. Percent Ag-experienced fractions displayed in Fig. 5 included all cells not falling into the naïve gate (i.e. CD45RA^{+}CCR7^{-} and CD45RA^{-}CCR7$^{+/-}$). (**D-E**) The final readout of MMr^{+} cells and naïve fractions is shown for healthy donor #H020W.

A

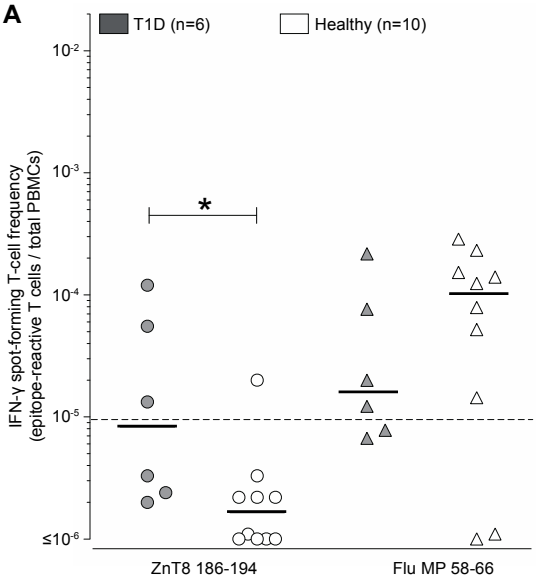

B

	% positive		T1D (n=6)						Healthy (n=10)									
	T1D	Healthy	D001W	D004W	D008W	D014W	D027W	D028W	H005W	H006W	H015W	H015T	H017T	H314C	H316C	H297S	H356C	H372C
ZnT8 186-194	50.0% (3/6)	10.0% (1/10)	13.3	55.5	3.3	120.4	2.2	2.2	1.1	2.2	3.3	1.1	2.2	0.0	0.0	2.2	20.0	0.0
Flu MP 58-66	66.7% (4/6)	80.0% (8/10)	217.6	76.6	6.7	7.8	20.0	12.2	52.2	124.3	286.4	139.9	1.1	232.0	14.4	78.8	153.2	0.0
PHA	100% (6/6)	100% (10/10)	++++	++++	++++	++++	++++	++++	++++	++++	++++	++++	++++	++++	++++	++++	++++	++++
Basal+3SD			5.8	10.0	10.0	5.8	5.8	20.8	20.8	15.3	5.8	20.8	5.8	10.0	5.8	17.3	10.0	30.0
Basal+4SD			7.7	13.3	13.3	7.7	7.7	27.7	27.7	20.3	7.7	27.7	7.7	13.3	7.7	23.1	13.3	40.0
Basal+5SD			9.6	16.7	16.7	9.6	9.6	34.7	34.7	25.4	9.6	34.7	9.6	16.7	9.6	28.8	16.7	50.0
Basal			1.1	3.3	3.3	7.8	2.2	7.8	11.1	4.4	1.1	12.2	1.1	3.3	4.4	6.7	3.3	13.3

Fig. S8. IFN-γ secretion by ZnT8$_{186-194}$-reactive CD8$^+$ T cells. (**A**) T1D and healthy donors previously analyzed by *ex-vivo* MMr staining for whom sufficient PBMCs remained were further analyzed by IFN-γ ELISpot as described (*7*). Briefly, unfractionated PBMCs ($3x10^5$/well) were plated in triplicate in anti-IFN-γ antibody-coated ELISpot PVDF plates in the presence of 10 µM ZnT8$_{186-194}$ or Flu MP$_{58-66}$ peptide or DMSO vehicle diluted in AIM-V medium supplemented with 0.5 U/ml IL-7. After 18 h, plates were revealed with biotin-conjugated anti-IFN-γ antibodies (U-CyTech), alkaline phosphatase-conjugated streptavidin and NBT-BCIP substrate, and counted on a BioSys Bioreader 5000 Pro-SF. Results are expressed as frequencies of epitope-reactive T cells out of total PBMCs after subtraction of background responses in the presence of DMSO alone (which were $\leq 10^{-5}$ in all cases). The dotted line represents the median cut-off for a positive response, which was set at 3 SDs above the average background for each individual, as previously determined by receiver-operator characteristics analysis (*3*). **p*=0.03 by Mann-Whitney test. (**B**) The corresponding raw IFN-γ ELISpot counts. All values, including basal + nSD cutoffs, are expressed as spot-forming cells/10^6 PBMCs with baseline subtraction. Non-subtracted basal values (reactivities to DMSO) are shown in the last row of each column. Reactivities are ranked as low (between 3 and 4 SD, yellow), intermediate (between 4 and 5 SD, orange), and high (>5 SD, red). The percentage of T1D and healthy subjects positive for each epitope is indicated in the second and third column, respectively. PHA was used as a polyclonal positive control. ++++, off-scale ELISpot reading.

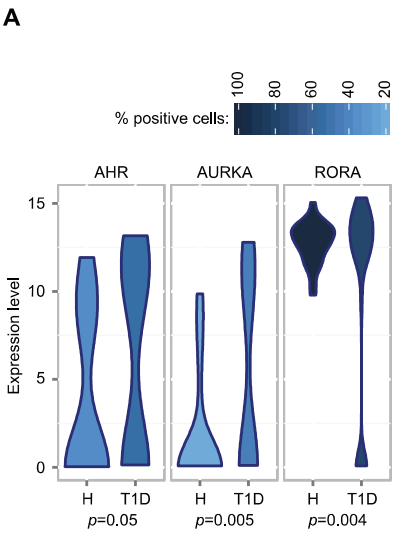

B

ID	TRBV	TRBJ	TRBD	CDR3	TRAV	TRAJ	CDR3
D004W					TRAV12-2*01/12-2*02/12-2*03	TRAJ15*01	CAVNQAGTALI
					TRAV27*01	TRAJ4*01	CAGDLESGGYNKLI
D007W	**TRBV19*01**/19*02/19*03	**TRBJ2-1*01**	**TRBD2*01**	CASSSGGGNEQFF	TRAV12-3*01/12-3*02	TRAJ33*01	CAMSAEGNYQLIW
	TRBV6-5*01	TRBJ1-3*01	TRBD2*02	CASSIGSGNTIYF			
D010W	**TRBV19*01**/19*02/19*03	TRBJ2-5*01	**TRBD2*01**	CASSIDGLASQETQYF			
	TRBV19*01/19*02/19*03	**TRBJ2-7*01**	TRBD2*02	CASSILAGGEQYF			
	TRBV28*01	TRBJ2-5*01	**TRBD1*01**	CASSHPDSQETQYF			
D011W	**TRBV9*01**/9*02/9*03	**TRBJ2-1*01**	TRBD2*02	CASSVGGRREQFF			
					TRAV29	TRAJ49*01	CAASIRSWGNQFYF
D013W	TRBV7-9*01/7-9*02/7-9*03	TRBJ1-4*01	**TRBD1*01**	CASVKGGMSEKLFF			
					TRAV12-2*01/12-2*02/12-2*03	TRAJ30*01	CAVKDDKIIF
					TRAV12-1*01	TRAJ8*01	CVVTYIQKLVF
D014W	TRBV7-9*01/7-9*02/7-9*03	**TRBJ2-1*01**	**TRBD1*01**	CASSLGPVQNSYNEQFF			
	TRBV7-9*01/7-9*02/7-9*03	**TRBJ2-3*01**	**TRBD1*01**	CASSSRYMRDADTQYF			
	TRBV27*01	**TRBJ2-7*01**	**TRBD1*01**	CASSFGNSYEQYF	**TRAV29**	TRAJ30*01	CAAIGNRDDKIIF
D016W					TRAV34*01	**TRAJ20*01**	CGANDYKLSF
D026W	**TRBV19*01**/19*02/19*03	TRBJ1-5*01	**TRBD1*01**	CASSIGQGSQPQHF	TRAV1-2*01	TRAJ33*01	CASKDSNYQLIW
	TRBV28*01	**TRBJ1-2*01**	TRBD2*02	CASSFGDGYTF			
					TRAV1-1*01/1-1*02	TRAJ28*01	FAVWGEGAGSYQLTF
D028W					TRAV16*01	TRAJ4*01	CAPLSGGYNKLIF
H002W	**TRBV9*01**/9*02/9*03	TRBJ1-3*01	**TRBD2*01**	CASSVAYRGTGNTIYF			
	TRBV28*01	**TRBJ2-1*01**	**TRBD1*01**	CASNLRDTGNEQFF	**TRAV35*02**	**TRAJ40*01**	CAPRTTSGTYKYI
H003W	TRBV16*01/16*02/16*03	TRBJ2-6*01	**TRBD2*01**	CASSLGGVIYNVLTF			
	TRBV2*01/2*02/2*03	TRBJ1-1*01	TRBD2*02	CASSDEGPPEAFF			
	TRBV13*01/13*02	**TRBJ1-2*01**	**TRBD1*01**	CASSHGTVTYGYTF			
H006W					TRAV21*01/21*02	**TRAJ57*01**	CAVRKPKTQGGSEKLV
H015W					TRAV12-2*01/12-2*02/12-2*03	TRAJ6*01	CAPQSGGSYIPTF
	TRBV18*01	**TRBJ2-7*01**	TRBD2*02	CASYPGTSGSYEQYF	TRAV41*01	TRAJ48*01	CAVRSDGNEKLT
H022W					TRAV12-2*01/12-2*02/12-2*03	TRAJ45*01	CAVNGGGADGLTF
					TRAV12-2*01/12-2*02/12-2*03	TRAJ52*01	CPVQGGGTSYGKLTF
					TRAV12-2*01/12-2*02/12-2*03	TRAJ37*01	CAVNLVRTGKLI
	TRBV28*01	**TRBJ2-1*01**	**TRBD2*01**	CASSFGNEQFF	TRAV16*01	**TRAJ36*01**	CAPTGANNL
H023W	TRBV7-9*01/7-9*02/7-9*03	**TRBJ1-2*01**	**TRBD1*01**	CASSMRQPGYTF			
					TRAV12-2*01/12-2*02/12-2*03	TRAJ52*01	CAVGGGGTSYGKLT
					TRAV12-2*01/12-2*02/12-2*03	TRAJ24*02	CDASPDSWGKLQ
H024W	**TRBV19*01**/19*02/19*03	**TRBJ2-7*01**	**TRBD1*01**	CASSAGQGAYEQYF			

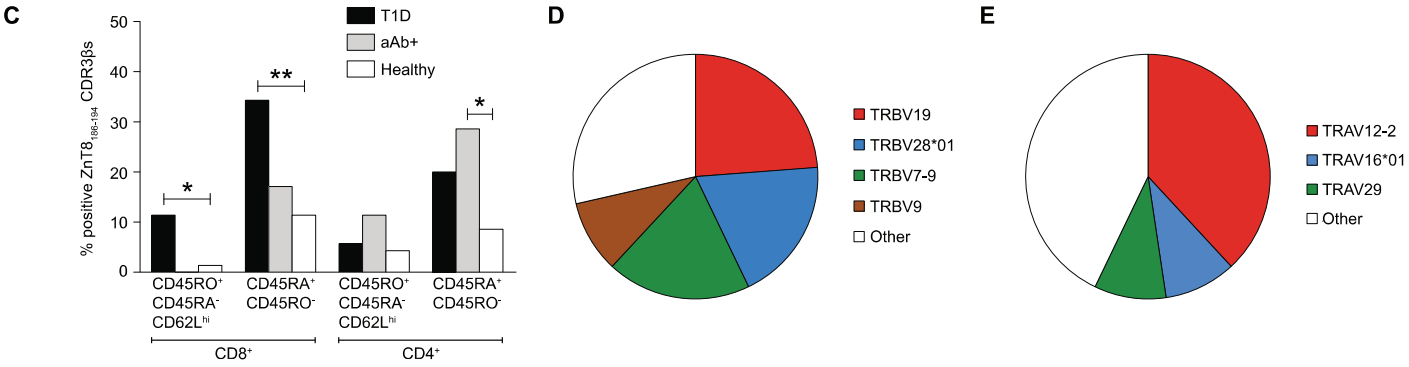

Fig. S9. Gene expression in *ex-vivo* single-sorted ZnT8$_{186\text{-}194}$ MMr^{+}CD8^{+} T cells. (**A**) Genes differentially expressed in individual ZnT8$_{186\text{-}194}$ MMr^{+}CD8^{+} T cells from T1D and healthy subjects. Single cells were sorted into empty PCR wells. cDNA synthesized with a Superscript VILO RT Kit (Invitrogen) was preamplified for 16 cycles with TATAA GrandMaster Mix and 61 primer pairs (Table S6) as follows: 1x [95°C 8 min], 16x [95°C 45 sec, 49°C 1 min (with 0.3°C increment/cycle), 72°C 1.5 min], 1x [72°C 7 min]. RT-PCR was carried out on a Fluidigm BioMark HD with the 96.96 Dynamic Array IFC, the GE 96x96 Fast PCR+ Melt protocol and SsoFast EvaGreen Supermix with Low ROX (Biorad), with 5 µM primers per assay. Data were analyzed using Fluidigm Real-Time PCR software followed by KNIME 2.5.2 and R 3.2.2 (www.r-project.org). Pre-processing *via* a linear model to correct for confounding effects was performed as described (*43*). The semi-continuous Hurdle model was subsequently applied to account for bimodal gene expression in single cells, allowing assessment of differential expression with respect to both the frequency of expression and the positive expression means *via* a likelihood ratio test. Violin plots display the density of expression (max.Ct–Ct) of genes that differ significantly between T1D and healthy donors (n=32 and n=25 ZnT8$_{186\text{-}194}$ MMr^{+}CD8^{+} T cells from 11 and 6 individuals, respectively). Blue shading illustrates the proportion of positive cells. *p* values were calculated with the Hurdle model. (**B**) *TRB* and *TRA* gene usage and the corresponding CDR3 aminoacid sequences of single-sorted cells from T1D (top, D-coded IDs) and healthy donors (bottom, H-coded IDs). Each line corresponds to an individual T cell. *TRBV* and *TRAV* genes shared with ZnT8$_{186\text{-}194}$-reactive clones obtained from separate subjects are shown in bold; repeatedly used genes are shown in color. (**C**) Prevalence of the CDR3β aminoacid sequences obtained from single-sorted cells among HLA-A2^{+} T1D (n=5), aAb^{+} (n=5) and healthy subjects (n=10), as assessed by *in-silico* analysis of CDRβ repertoires obtained from the indicated CD8^{+} and CD4^{+} T-cell subsets. *$p\leq0.04$, **$p=0.008$ by Fisher's exact test. (**D-E**) Distribution of *TRBV* (D) and *TRAV* (E) gene usage among ZnT8$_{186\text{-}194}$ MMr^{+}CD8^{+} T cells. Color codes are matched to panel B.

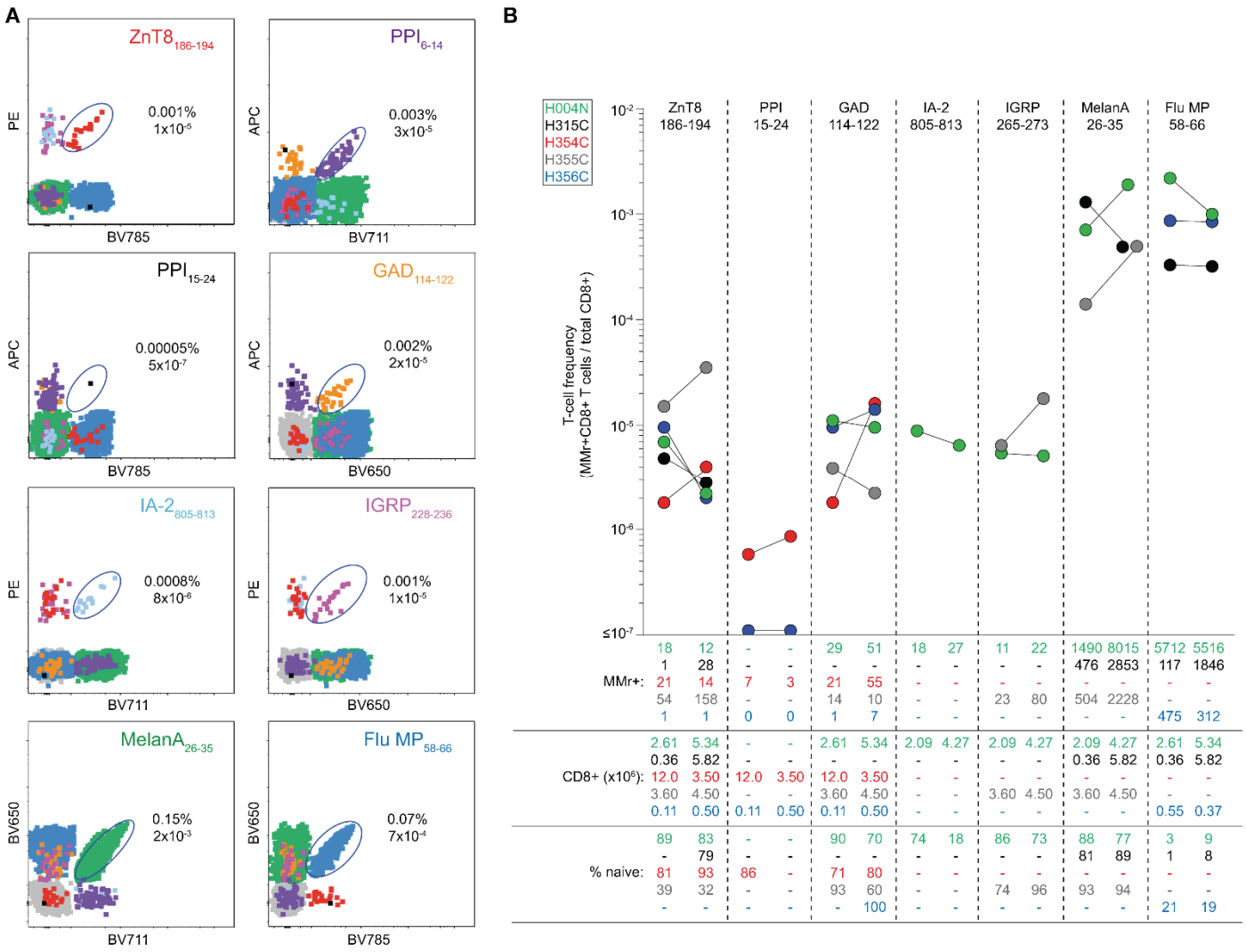

Fig. S10. Extended combinatorial MMr panel for the analysis of multiple islet-reactive CD8$^+$ T-cell populations, and reproducibility of *ex-vivo* MMr assays. (**A**) After magnetic depletion of CD8$^-$ cells, PBMCs were sequentially gated as depicted in Fig. S7 and the indicated MMr$^+$ populations were visualized using the gating strategy previously detailed for combinatorial MMr staining (*9*) and the FlowJo v10 software. The staining panel also included Live/Dead Aqua, anti-CD3-APC-H7 (clone SK7, BD), anti-CD8-PE-Cy7 (clone SK1, eBioscience), anti-CD45RA-FITC (clone HI100, eBioscience) and anti-CCR7-BV421 (clone 150503, BD). The final readout obtained for T1D patient D322D after gating out events positive for <2 or >2 MMr fluorochromes is shown, with events corresponding to each epitope-reactive population depicted in different colors within each plot, and MMr$^-$ events depicted in grey. (**B**) Reproducibility between the 3-MMr panel depicted in Fig. S7 and the extended 8-MMr panel presented here. Separate blood draws from 5 subjects (H004N, green; H315C, black; H354C, red; H355C, grey; H356C, blue) were analyzed with both panels and the frequency counts were compared. The corresponding MMr$^+$ and total CD8$^+$ T-cell counts (x10^6) are indicated with the same color code below each distribution, together with the percentage of naïve (CD45RA$^+$CCR7$^+$) cells in each MMr$^+$ fraction (for fractions ≥5 MMr$^+$ cells).

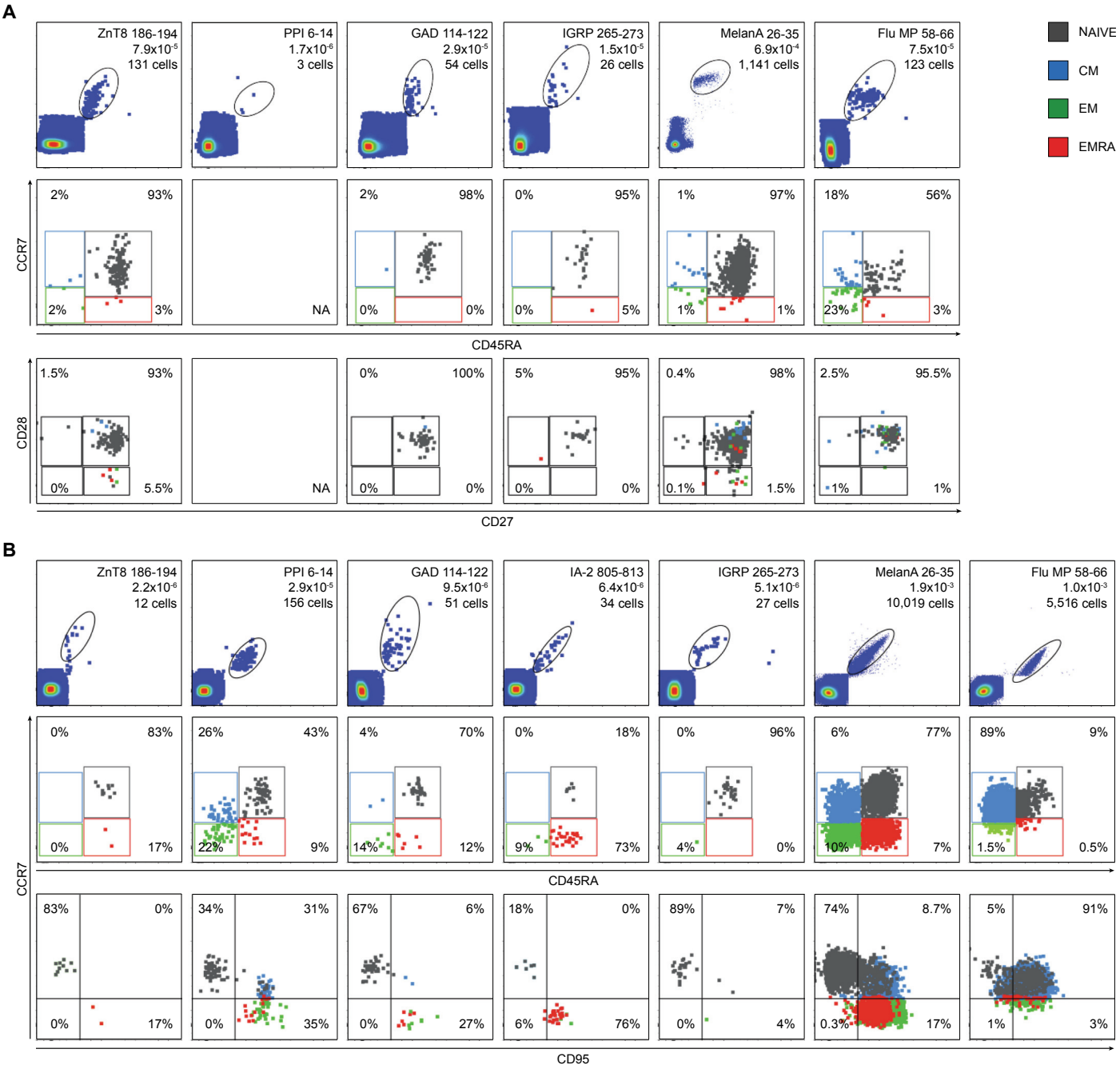

Fig. S11. CD27, CD28 and CD95 expression on ZnT8$_{186-194}$-reactive CD8$^+$ T cells. (**A**) Representative CD27/CD28 staining of MMr$^+$CD8$^+$ T cells from subject H372C. The first row depicts the fraction of MMr$^+$ cells for each of the indicated epitopes. The corresponding frequency out of the total 1.7x10^6 CD8$^+$ T cells acquired and the number of MMr$^+$ events counted are indicated. The second row shows the percent distribution of naïve (CD45RA$^+$CCR7$^+$; grey), central memory (CM, CD45RA$^-$CCR7$^+$; blue), effector memory (EM, CD45RA$^-$CCR7$^-$; green) and terminally differentiated EM CD45RA$^+$ cells (EMRA, CD45RA$^+$CCR7$^-$; red) within each MMr$^+$ fraction. The third row depicts CD27 (AlexaFluor700-labeled clone O323, eBioscience) and CD28 expression (BV421-labeled clone CD28.2, BioLegend) within each of these subsets, using the same color code, with total percent cells indicated in each quadrant. NA, not available (<5 MMr$^+$ events counted). (**B**) Representative CD95 staining (PE/CF594-labeled clone DX2, BD) for MMr$^+$CD8$^+$ T cells from subject H004N. A total of 5.3x10^6 CD8$^+$ T cells was acquired, and data are represented as in panel A. Results are representative of 4 subjects tested.

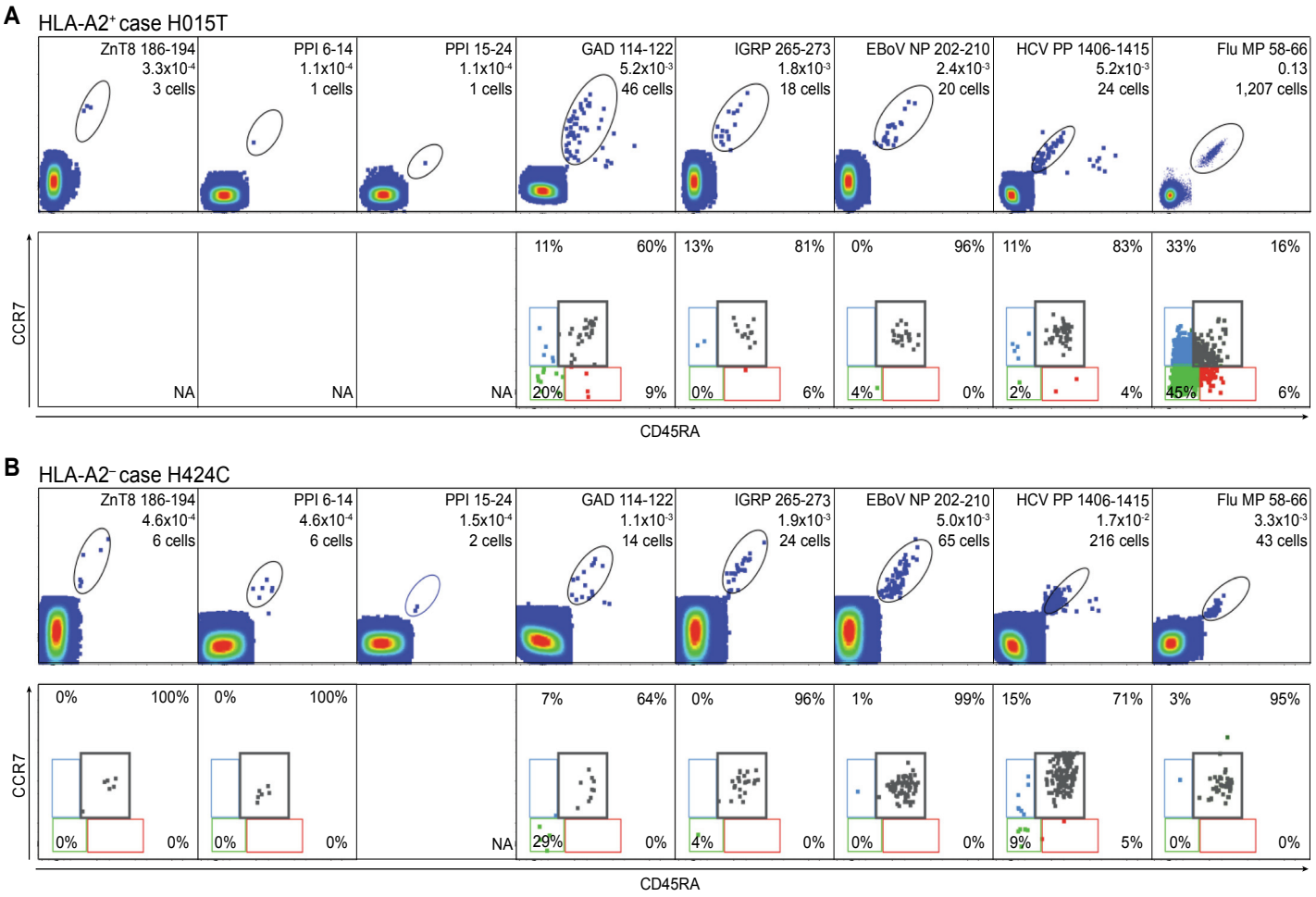

Fig. S12. Representative MMr and CD45RA/CCR7 dot plots for HLA-A2$^+$ and HLA-A2$^-$ healthy donors depicted in Fig. 6F-G. (**A**) MMr (top row) and CD45RA/CCR7 staining (bottom row) for each of the indicated epitopes for HLA-A2$^+$ case H015T. The corresponding frequency out of the total 0.9x10^6 CD8$^+$ T cells acquired and the number of MMr$^+$ events counted are indicated in the top row. The second row shows the percent distribution of naïve (CD45RA$^+$CCR7$^+$; grey), central memory (CD45RA$^-$CCR7$^+$; blue), effector memory (CD45RA$^-$CCR7$^-$; green) and terminally differentiated EM CD45RA$^+$ cells (CD45RA$^+$CCR7$^-$; red) within each MMr$^+$ fraction, with percent cells indicated in each quadrant. NA, not available (<5 MMr$^+$ events counted). (**B**) The same representation is shown for HLA-A2$^-$ case H424C. A total of 1.3x10^6 CD8$^+$ T cells was acquired.

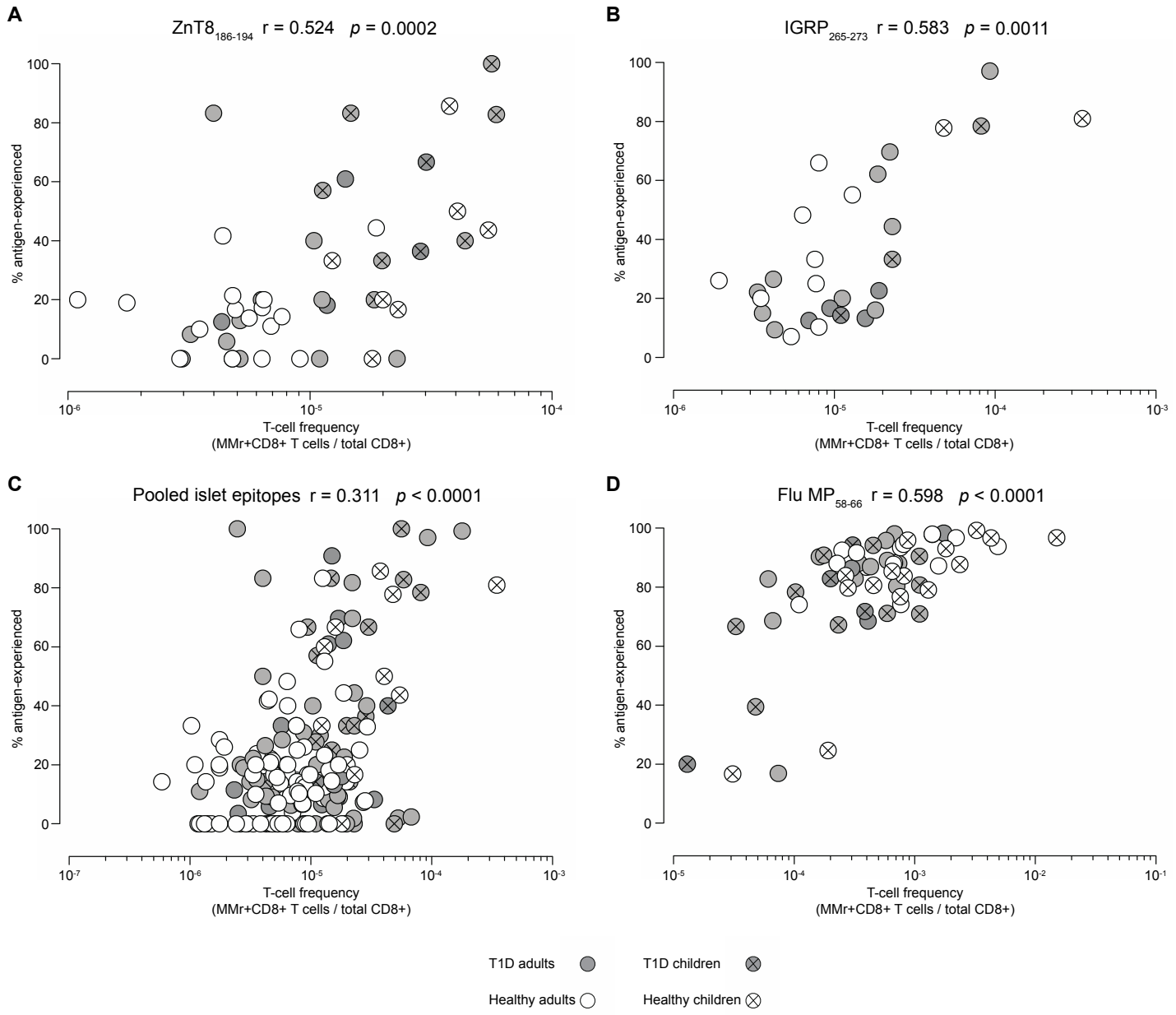

Fig. S13. Correlation between the frequency of MMr^+CD8^+ T cells and the Ag-experienced fraction within the same MMr^+CD8^+ population. (**A**) Correlation for $ZnT8_{186-194}$ MMr^+CD8^+ T cells. (**B**) Correlation for $IGRP_{265-273}$ MMr^+CD8^+ T cells. (**C**) Correlation for pooled MMr^+CD8^+ T cells recognizing all islet epitopes analyzed ($ZnT8_{186-194}$, PPI_{6-14}, PPI_{15-24}, $GAD_{114-122}$, IA-$2_{805-813}$, $IGRP_{265-273}$). (**D**) Correlation for Flu MP_{58-66} MMr^+CD8^+ T cells. Graphs were obtained by compiling data presented in Fig. 5 for T1D patients (adults, grey circles; children, crossed grey circles) and age/sex-matched healthy donors (adults, white circles; children, crossed white circles). Values obtained by Spearman correlation analysis are shown for each graph.

Status	Donor	Age (yrs)	Gender (M/F)	T1D duration (days)	GADA	IA-2A	ZnT8A	Therapy	Sort strategy	Sorted wells	Growing wells	ZnT8 MMr+ wells	Cloning efficiency	Clones	Source cell
T1D	D222D	60	M	3	+	-	+	Insulin	In vitro	100	5	3	3%	(1)	ND
														2	ND
														3	ND
T1D	D010R	12	M	8	-	+	-	Insulin	Ex vivo	50	10	2	4%	1D3	$CD45RA^+CCR7^+$
														(1E2)	$CD45RA^+CCR7^+$
T1D	D349V	62	F	6	+	+	+	Insulin	Ex vivo	67	1	1	1%	178B9	$CD45RA^+CCR7^+$
T1D	D267T	25	F	12	+	ND	-	Insulin	Ex vivo	50	7	1	2%	33B8	$CD45RA^+CCR7^+$
T1D	D351D	32	M	57	+	-	-	Insulin	Ex vivo	132	6	3	2%	188C3	$CD45RA^+CCR7^+$
														188D3	$CD45RA^+CCR7^+$
H	H017N	34	F	NA	-	-	-	None	In vitro	80	8	1	1%	A1	ND
H	H314C	24	M	NA	-	-	ND	None	Ex vivo	60	2	1	2%	6C4	$CD45RA^+CCR7^+$
H	H328C	29	M	NA	-	-	ND	None	Ex vivo	45	12	0	0%	NA	NA
									In vitro	119	26	3	2%	8E8	ND
														9C8	ND
														9B3	ND
H	H079O	35	F	NA	-	-	-	None	Ex vivo	260	7	1	0.4%	42D8	$CD45RA^+CCR7^+$
H	H034O	43	F	NA	-	-	-	None	Ex vivo	80	1	1	1%	141B9	ND

Table S1. Summary of $ZnT8_{186\text{-}194}$-reactive $CD8^+$ T-cell clones. Clones in parentheses could not be stabilized in long-term cultures and underwent more limited characterization. For those clones obtained after *ex-vivo* index sorting of $ZnT8_{186\text{-}194}$ MMr^+ cells, the surface phenotype of the source cell is indicated in the last column. NA, not applicable; ND, not determined; GADA, GAD aAbs; IA-2A, IA-2 aAbs; ZnT8A, ZnT8 aAbs.

Study group	Case ID	Age (years)	Gender (M/F)	T1D duration (Months)	HLA-A*02 status	IAA	GADA	IA-2A	ZnT8A	Therapy
T1D (n=10)	jdrfT1D1	21	M	3.6	-	+	+	+	+	Insulin
	jdrfT1D2	38	M	17.7	-	+	+	+	+	Insulin
	jdrfT1D3	50	F	34.6	-	+	+	-	-	Insulin
	sbirT1D3	25	M	25.7	-	+	-	+	-	Insulin
	sbirT1D4	44	M	10.2	-	-	-	-	-	Insulin
	sbirT1D5	16	M	17.2	+	-	-	-	-	Insulin
	sbirT1D6	20	F	15.4	+	+	+	-	-	Insulin
	sbirT1D7	25	F	10.7	+	-	+	+	+	Insulin
	sbirT1D8	41	M	8.3	+	-	+	-	-	Insulin
	sbirT1D9	17	M	8.3	+	+	+	-	-	Insulin
At-risk (n=7)	jdrfAB+ 2	44	F	NA	+	+	-	-	-	None
	jdrfAB+ 3	59	M	NA	-	+	+	-	-	None
	jdrfAB+ 4	29	M	NA	+	-	+	+	-	None
	jdrfAB+ 5	49	F	NA	+	-	+	+	-	None
	jdrfAB+ 6	53	M	NA	+	-	+	+	+	None
	jdrfAB+ 7	32	F	NA	-	-	+	-	-	None
	jdrfAB+ 9	17	F	NA	+	-	+	+	+	None
Healthy (n=12)	control1	24	F	NA	+	-	-	-	-	None
	control2	38	F	NA	-	-	-	-	-	None
	control3	22	F	NA	+	-	-	-	-	None
	sbirControl1	27	F	NA	+	-	-	-	-	None
	sbirControl3	22	M	NA	+	-	-	-	-	None
	sbirControl4	27	M	NA	+	-	-	-	-	None
	sbirControl5	25	F	NA	+	-	-	-	-	None
	sbirControl6	40	M	NA	+	-	-	-	-	None
	sbirControl7	33	M	NA	-	-	-	-	-	None
	sbirControl8	37	M	NA	+	-	-	-	-	None
	sbirControl9	21	M	NA	+	-	-	-	-	None
	sbirControl10	35	M	NA	+	-	-	-	-	None

Table S2. Characteristics of study subjects for *in-silico TRB* analyses. IAA, insulin aAbs; NA, not applicable.

Pediatric subjects - T1D

Case ID	Age (years)	Gender (M/F)	T1D duration (Months)	IAA	GADA	IA-2A	ZnT8A	Therapy
D001W	13	F	18	+	-	-	-	Insulin
D004W	15	F	13	ND	+	+	+	Insulin
D007W	10	F	30	ND	+	+	+	Insulin
D008W	11	M	6	ND	+	+	+	Insulin
D009W	10	F	5	ND	+	+	+	Insulin
D010W	17	M	15	ND	+	+	+	Insulin
D011W	10	M	5	ND	+	+	+	Insulin
D013W	10	M	13	ND	+	-	+	Insulin
D014W	14	M	18	ND	+	+	+	Insulin
D016W	18	M	19	ND	+	-	+	Insulin
D019W	8	M	12	+	-	-	-	Insulin
D027W	10	M	23	ND	+	+	+	Insulin
D028W	13	M	24	ND	-	+	+	Insulin
D001R	8	F	0.2	-	+	+	ND	Insulin
D006R	14	M	0.3	+	-	-	ND	Insulin
D016R	12	F	0.3	ND	+	-	ND	Insulin
N=16	**12**	**38% F**	**15**		**75% +**	**63% +**	**85% +**	**100% insulin**
	8-18	**62% M**	**0.2-24**		**25% -**	**37% -**	**15% -**	

Adult subjects - T1D

Case ID	Age (years)	Gender (M/F)	T1D duration (Months)	IAA	GADA	IA-2A	ZnT8A	Therapy
D015H	24	F	0.2	ND	+	+	+	Insulin
D026W	23	M	6.0	ND	+	+	+	Insulin
D267T	25	F	0.4	ND	+	ND	-	Insulin
D291V	33	M	0.2	ND	+	+	+	Insulin
D292V	28	M	0.6	ND	-	+	ND	Insulin
D296D	25	F	0.1	ND	+	+	ND	Insulin
D307D	23	M	1.2	ND	-	+	ND	Insulin
D322D	31	M	0.2	ND	+	+	+	Insulin
D323D	48	M	0.2	ND	-	-	-	Insulin
D324D	28	F	2.6	ND	+	+	+	Insulin
D328V	26	F	0.2	-	+	-	+	Insulin
D329D	23	M	0.1	ND	+	+	-	Insulin
D330D	25	F	0.1	ND	+	-	+	Insulin
D338D	31	M	0.3	ND	+	+	+	Insulin
D339V	29	M	0.1	ND	+	+	+	Insulin
D347D	42	M	1.0	ND	+	+	+	Insulin
D349D	62	F	0.2	ND	+	+	+	Insulin
D350D	44	F	0.2	ND	-	+	-	Insulin
D351D	32	M	1.9	ND	+	-	-	Insulin
D354V	54	F	0.2	ND	+	+	+	Insulin
D355D	28	M	0.2	ND	+	+	+	Insulin
D359D	25	F	0.2	ND	+	+	+	Insulin
D363V	58	F	0.4	ND	+	+	-	Insulin
N=23	**28**	**48% F**	**0.2**		**83% +**	**82% +**	**70% +**	**100% insulin**
	23-62	**52% M**	**0.1-6**		**17% -**	**18% -**	**30% -**	

Pediatric subjects - Healthy

H003W	11	M	NA	ND	-	-	-	None
H005W	17	M	NA	ND	-	-	-	None
H006W	10	F	NA	ND	-	-	-	None
H012W	10	M	NA	ND	-	-	-	None
H015W	13	M	NA	ND	-	-	-	None
H017W	13	F	NA	ND	-	-	-	None
H018W	9	M	NA	ND	-	-	-	None
H020W	14	M	NA	ND	-	-	-	None
H021W	12	F	NA	ND	-	-	-	None
H022W	11	M	NA	ND	-	-	-	None
H023W	10	M	NA	ND	-	-	-	None
H024W	17	M	NA	ND	-	-	-	None
H025W	10	F	NA	ND	-	-	-	None
H095M	14	M	NA	ND	ND	ND	ND	None
H100M	13	M	NA	ND	ND	ND	ND	None
H103M	16	F	NA	ND	ND	ND	ND	None
H113M	11	F	NA	ND	ND	ND	ND	None
N=17	**12**	**35% F**			**0% +**	**0% +**	**0% +**	**100% none**
	9-17	**65% M**			**100% -**	**100% -**	**100% -**	

Adult subjects - Healthy

H002W	23	M	NA	ND	-	-	-	None
H004N	42	M	NA	-	-	-	ND	None
H005N	36	F	NA	-	-	-	ND	None
H015T	30	M	NA	-	-	-	ND	None
H017N	34	F	NA	ND	-	ND	-	None
H034O	43	F	NA	-	-	-	ND	None
H079O	35	F	NA	-	-	-	ND	None
H087N	33	M	NA	-	-	-	ND	None
H109S	64	M	NA	ND	ND	ND	ND	None
H170S	37	F	NA	ND	-	ND	ND	None
H297S	27	M	NA	ND	-	ND	ND	None
H312C	34	M	NA	ND	-	ND	ND	None
H314C	24	M	NA	ND	ND	ND	ND	None
H315C	40	F	NA	ND	-	ND	ND	None
H316C	25	F	NA	ND	ND	ND	ND	None
H321C	30	F	NA	ND	ND	ND	ND	None
H328C	29	M	NA	ND	ND	ND	ND	None
H333O	23	M	NA	ND	ND	ND	ND	None
H353C	40	M	NA	ND	-	ND	ND	None
H354C	25	F	NA	ND	-	ND	ND	None
H356C	26	M	NA	ND	-	ND	ND	None
H372C	22	F	NA	ND	ND	ND	ND	None
N=22	**32**	**45% F**						**100% none**
	22-64	**55% M**						

Table S3. Characteristics of HLA-A2$^+$ study subjects for *ex-vivo* MMr studies. Individual clinical profiles of T1D pediatric subjects (top left; n=16), age/sex-matched healthy pediatric subjects (bottom left; n=17), T1D adults (top right; n=23) and age/sex-matched healthy adults (bottom right; n=22) are shown along with their distribution within each group (median and range for numerical variables). ND, not determined; NA, not applicable.

Case ID	Age (yrs)	Gender (M/F)	HLA-A/B	Predicted HLA binding affinity (nM)							
				ZnT8 186-194	PPI 6-14	PPI 15-24	GAD 114-122	IGRP 265-273	EboV NP 202-210	HCV PP 1406-1415	Flu MP 58-66
H015T ▽	32	M	A*02:01	355	13	234	23	16	10	41	16
			NA	–	–	–	–	–	–	–	–
			NA	–	–	–	–	–	–	–	–
			NA	–	–	–	–	–	–	–	–
H311C ○	33	M	A*02:01	355	13	234	23	16	10	41	16
			A*01:01	14759	19182	33558	7213	19192	16505	26256	22016
			B*15:01	10716	2679	6813	4816	1290	2288	2251	12092
			B*44:02	25029	17913	25941	18087	18349	14949	27487	24697
H314C ◇	24	M	A*02:01	355	13	234	23	16	10	41	16
			A*68:01	15512	29930	43713	31674	22468	26846	35191	22471
			B*07:02	7498	7405	17414	28460	11781	3812	6075	16630
			B*44:02	25029	17913	25941	18087	18349	14949	27487	24697
H356C □	28	M	A*02:01	355	13	234	23	16	10	41	16
			A*01:01	14759	19182	33558	7213	19192	16505	26256	22016
			B*08:01	12180	5071	31975	15488	14954	4951	17633	11752
			B*49:01	NA	NA	NA	NA	NA	NA	NA	NA
H372C △	24	F	A*02:01	355	13	234	23	16	10	41	16
			A*26:01	21758	23637	36297	23966	20711	23427	26585	19347
			B*18:01	21582	17880	39939	23844	13228	21410	33037	19695
			B*44:02	25029	17913	25941	18087	18349	14949	27487	24697
H018N ▽	35	F	A*02:05	NA	NA	NA	NA	NA	NA	NA	NA
			A*30:02	10619	2111	12271	2619	5559	1870	9148	11631
			B*18:01	21582	17880	39939	23844	13228	21410	33037	19695
			B*50:01	NA	NA	NA	NA	NA	NA	NA	NA
H279S ■	33	M	A*01:01	14759	19182	33558	7213	19192	16505	26256	22016
			A*66:01	9110	11692	39995	18633	9799	10023	37091	8751
			B*08:01	12180	5071	31975	15488	14954	4951	17633	11752
			B*41:02	NA	NA	NA	NA	NA	NA	NA	NA
H355C ●	34	M	A*03:01	18409	4379	15490	11720	6945	1985	9370	15303
			A*24:02	12287	1678	34034	18766	3617	41	36129	7558
			B*07:02	7498	7405	17414	28460	11781	3812	6075	16630
			B*35:02	NA	NA	NA	NA	NA	NA	NA	NA
H423C ◆	24	M	A*03:01	18409	4379	15490	11720	6945	1985	9370	15303
			A*23:01	11384	968	36359	17176	5503	100	32936	6184
			B*07:02	7498	7405	17414	28460	11781	3812	6075	16630
			B*15:01	10716	2679	6813	4816	1290	2288	2251	12092
H424C ▲	28	F	A*32:01	2093	727	35528	11017	32	12	9322	82
			A*32:01	2093	727	35528	11017	32	12	9322	82
			B*44:02	25029	17913	25941	18087	18349	14949	27487	24697
			B*44:02	25029	17913	25941	18087	18349	14949	27487	24697

Table S4. Characteristics of HLA-A2^{+} and HLA-A2^{-} healthy donors for *ex-vivo* MMr studies. Predicted HLA Class I peptide binding affinities were calculated using NetMHC 4.0 (http://www.cbs.dtu.dk/services/NetMHC/). HLA-A2 (A*02:01) and predicted affinity values compatible with peptide binding to the indicated HLA allotypes are highlighted in red. NA, not available.

	nPOD case	Sex	Age (yrs)	T1D T2D (yrs)	Positive aAbs	C-peptide (ng/ml)	ZnT8 MMr+		MelanA MMr+		CDR3β+
							Pa	PLN	Pa	PLN	PLN
T1D (n=9)	6070	F	23	7	IA-2/mIAA	<0.05	74	0	0	NA	NA
	6161	F	19	7	IA-2/mIAA	<0.05	124	1176	0	0	8-18-0
	6211	F	24	4	GAD/IA-2/ZnT8/mIAA	<0.05	30	60	0	54	0-0-0
	6212	M	20	5	mIAA	<0.05	0	0	NA	NA	14-0-0
	6237	F	18	12	GAD/mIAA	<0.05	267	0	0	NA	NA
	6242	M	39	19	IA-2/mIAA	<0.05	66	101	0	0	0-0-5
	6243	M	13	5	mIAA	0.42	0	209	NA	0	0-0-0
	6258	F	39	37	mIAA	<0.05	118	299	0	0	NA
	6325	F	20	6	GAD/IA-2	0.14	28	0	0	0	NA
aAb+ (n=9)	6080	F	69	NA	GAD/mIAA	1.84	55	50	25	61	NA
	6101	M	65	NA	GAD	26.18	0	0	NA	NA	NA
	6123	F	23	NA	GAD	2.01	0	0	NA	NA	NA
	6151	M	30	NA	GAD	5.49	28	NA	0	NA	NA
	6154	F	49	NA	GAD	<0.05	64	NA	0	NA	NA
	6171	F	4	NA	GAD	8.95	37	0	0	NA	NA
	6347	M	9	NA	mIAA	3.26	33	60	0	191	NA
	6388	F	25	NA	GAD/mIAA	1.38	34	35	0	0	NA
	6397	F	21	NA	GAD	12.8	42	189	0	0	NA
No diabetes (n=11)	6103	M	2	NA	—	0.98	55	0	0	NA	NA
	6179	F	20	NA	—	2.74	96	150	0	0	NA
	6182	M	3	NA	—	2.28	23	163	0	65	NA
	6227	F	17	NA	—	2.75	3	0	0	NA	NA
	6234	F	20	NA	—	6.89	6	0	0	NA	NA
	6254	M	38	NA	—	6.43	0	0	NA	NA	0-4-0
	6271	M	17	NA	—	11.47	0	0	NA	0	0-0-0
	6287	F	57	NA	—	4.75	4	0	0	NA	9-0-0
	6289	M	19	NA	—	8.05	0	0	NA	NA	0-0-0
	6357	M	5	NA	—	8.82	0	0	NA	NA	NA
	6366	F	21	NA	—	0.41	0	0	NA	NA	NA
T2D (n=3)	6028	M	33	17	—	22.40	0	0	NA	NA	NA
	6059	F	19	0.3	—	10.68	0	107	NA	0	NA
	6275	M	48	2	—	3.46	0	0	NA	NA	0-2-0
Other	6288	M	55	NA	—	12.96	211	87	0	0	250-0-0

Table S5. Characteristics of nPOD cases for *in-situ* ZnT8$_{186\text{-}194}$ MMr staining. The clinical caracteristics of each case are reported along with the counts (x10^{-3}) of ZnT8$_{186\text{-}194}$ and MelanA$_{26\text{-}35}$ MMr^{+} cells/mm^{2} pancreas (Pa) and PLN section area. Positive sections are marked in red. In several cases, the PLN CD8^{+} T-cell repertoire was interrogated *in-silico* for the presence of immunodominant CDR3β aminoacid sequences retrieved from 3 ZnT8$_{186\text{-}194}$-reactive CD8^{+} T-cell clones (Fig. 4D). The results of this *in-silico* search are reported in the last column, with numbers indicating the frequency of the 3 selected sequences (D010R 1E2, H034O 141B9 and H328C 8E8, respectively) per 10^{6} TCRs, and positive counts indicated in red. Case #6287 (presenting a circumscribed neuroendocrine tumor in the pancreatic pan-

body region; pan-tail region analyzed here) was classified as a non-diabetic control, while non-diabetic case #6288 was classified as ‘other’ based on a history of non-alcoholic cirrhosis and histological findings of chronic pancreatitis. NA, not applicable or not available; mIAA, micro-insulin aAbs.

Preamplification		qPCR	
INFg-1_3'	TGGATGCTCTGGTCATCTTT	INFg-1_3'	TGGATGCTCTGGTCATCTTT
INFg-1_5'	CTGTTACTGCCAGGACCCAT	INFg-2_5'	GGTCATTCAGATGTAGCGGA
IL4_1_3'	CTCTGGTTGGCTTCCTTCAC	IL4_1_3'	CTCTGGTTGGCTTCCTTCAC
IL4_1-5'	TGCCTCCAAGAACACAACTG	IL4_2-5'	GGCAGTTCTACAGCCACCAT
IL10n2_1-3'	GCCTTGCTCTTGTTTTCACAG	IL10n2_1-3'	GCCTTGCTCTTGTTTTCACAG
IL10n2_1-5'	TGCTGGAGGACTTTAAGGGTTA	IL10n2_2-5'	TTTAAGGGTTACCTGGGTTGC
IL-13-1_3'	TTTACAAACTGGGCCACCTC	IL-13-1_3'	TTTACAAACTGGGCCACCTC
IL-13-1_5'	GGTCAACATCACCCAGAACC	IL-13_2_5'	GTACTGTGCAGCCCTGGAAT
Il17F_1-3'	ATGCAGCCCAAGTTCCTACA	Il17F_1-3'	ATGCAGCCCAAGTTCCTACA
Il17F_1-5'	TCCAAAAGCCTGAGAGTTGC	Il17F_2-5'	GCCTGTGCCAGGAGGTAGTA
FOXp3n1-3'	GCGTGTGAACCAGTGGTAGAT	FOXp3n1-3'	GCGTGTGAACCAGTGGTAGAT
FOXp3n-1-5'	GTAGCCATGGAAACAGCACAT	FOXp3n2-5'	ACATTCCCAGAGTTCCTCCAC
SRP14_3'	GCTGCTGCTTTGGTCTTCTT	SRP14_5'-2	TACTGTGGAGGGCTTTGAGC
SRP14_5'	TATGACGGTCGAACCAAACC	SRP14_3'	GCTGCTGCTTTGGTCTTCTT
c-Maf_1-3'	GCTTCCAAAATGTGGCGTAT	c-Maf_1-3'	GCTTCCAAAATGTGGCGTAT
c-Maf_2-5'	GGACGCGTACAAGGAGAAAT	c-Maf_2-5'	GGACGCGTACAAGGAGAAAT
Egr2_1-3'	GTTGAAGCTGGGGAAGTGAC	Egr2_1-3'	GTTGAAGCTGGGGAAGTGAC
Egr2_2-5'	TGGAGAGAAGAGGTCGTTGG	Egr2_2-5'	TGGAGAGAAGAGGTCGTTGG
RORCnew_3-3'	TCCCTCTGCTTCTTGGACAT	RORCnew_3-3'	TCCCTCTGCTTCTTGGACAT
RORCnew_4-5'	TCCCGAGATGCTGTCAAGTT	RORCnew_4-5'	TCCCGAGATGCTGTCAAGTT
T-bet_1-3'	ATCTCCCCCAAGGAATTGAC	T-bet_1-3'	ATCTCCCCCAAGGAATTGAC
T-bet_2-5'	CCGTGACTGCCTACCAGAAT	T-bet_2-5'	CCGTGACTGCCTACCAGAAT
TGFb_1-3'	CACAACTCCGGTGACATCAAA	TGFb_5'-Taq-2	TACCTGAACCCGTGTTGCTT
TGFb_5'-Taq-1	TACCTGAACCCGTGTTGCT	TGFb_3'-Taq-1	CAACTCCGGTGACATCAAAA
CD127_1-3'	CTGCAGGAGTGTCAGCTTTG	CD127_1-3'	CTGCAGGAGTGTCAGCTTTG
CD127_1-5'	CTGAGGCTCCTTTTGACCTG	CD127_1-5'	CTGAGGCTCCTTTTGACCTG
CTLA-4_1-3'	GTTGCCTATGCCCAGGTAGT	CTLA-4_1-3'	GTTGCCTATGCCCAGGTAGT
CTLA-4_1-5'	TGACAGCCAGGTGACTGAAG	CTLA-4_2-5'	TGGGGAATGAGTTGACCTTC
GITR_3-3'	TGCAGTCTGTCCAAGGTTTG	GITR_3-3'	TGCAGTCTGTCCAAGGTTTG
GITR_3-5'	GAGTGGGACTGCATGTGTGT	GITR_3-5'	GAGTGGGACTGCATGTGTGT
HELIOS_1-3'	ATGGCCCCTGATCTCATCT	HELIOS_1-3'	ATGGCCCCTGATCTCATCT
HELIOS_2-5'	CGAAAGGGAGCACTCCAATA	HELIOS_2-5'	CGAAAGGGAGCACTCCAATA
ICOS_1-3'	TCGTGCACACTGGATGAATA	ICOS_1-3'	TCGTGCACACTGGATGAATA
ICOS_1-5'	GGACCATTCTCATGCCAACT	ICOS_2-5'	GGTTACCCATAGGATGTGCAG
CCR6_1-3'	CACCAGAATATTCCCCAGGA	CCR6_1-3'	CACCAGAATATTCCCCAGGA
CCR6_2-5'	TCAGCGATGTTTTCGACTCC	CCR6_2-5'	TCAGCGATGTTTTCGACTCC
CCR7_1-3'	ATAGGGAGGAACCAGGCTTT	CCR7_1-3'	ATAGGGAGGAACCAGGCTTT
CCR7_1-5'	CAATGAAAAGCGTGCTGGT	CCR7_2-5'	GTGGTGGCTCTCCTTGTCAT
IL-18_RAP_1-3'	GGTGAGAGTCGATTTCTGTGG	IL-18_RAP_1-3'	GGTGAGAGTCGATTTCTGTGG
IL-18_RAP_2-5'	TTGCAGGAGAGCGAATTAAA	IL-18_RAP_2-5'	TTGCAGGAGAGCGAATTAAA
TNF_1-3'	TGAGGTACAGGCCCTCTGAT	TNF_1-3'	TGAGGTACAGGCCCTCTGAT
TNF_1-5'	CCCCAGGGACCTCTCTCTAA	TNF_2-5'	CCCGAGTGACAAGCCTGTAG
IL21_1-3'	AAGCAGGAAAAAGCTGACCA	IL21_1-3'	AAGCAGGAAAAAGCTGACCA
IL21_2-5'	TCGCCACATGATTAGAATGC	IL21_2-5'	TCGCCACATGATTAGAATGC
CCR5_1-5'	GGCCATCTCTGACCTGTTTTT	CCR5_1-3'	AAACACAGCATGGACGACAG
CCR5_1-3'	AAACACAGCATGGACGACAG	CCR5_2-5'	GTCCCCTTCTGGGCTCACTA
RORA_4-3'	GGTCTGCCACGTTATCTGCT	RORA_4-3'	GGTCTGCCACGTTATCTGCT
RORA_4-5'	CACCAGCATCAGGCTTCTTT	RORA_4-5'	CACCAGCATCAGGCTTCTTT
GATA3_1-5'	CCGCCCTACTACGGAAACTC	GATA3_1-5'	CCGCCCTACTACGGAAACTC
GATA3_1-3'	TTGGAGAAGGGGCTGAGAT	GATA3_1-3'	TTGGAGAAGGGGCTGAGAT
IL17A_3-3'	CCGGTTATGGATGTTCAGGT	IL17A_3-3'	CCGGTTATGGATGTTCAGGT
IL17A_3-5'	TGGGAAGACCTCATTGGTGT	IL17A_3-5'	TGGGAAGACCTCATTGGTGT
IL9_1-3'	TGTTTGCATGGTGGTATTGG	IL9_1-3'	TGTTTGCATGGTGGTATTGG
IL9_2-5'	CTCATCAACAAGATGCAGGAAG	IL9_2-5'	CTCATCAACAAGATGCAGGAAG
IL22_1-3'	GTTCAGCACCTGCTTCATCA	IL22_1-3'	GTTCAGCACCTGCTTCATCA
IL22_2-5'	TCCAGCAGCCCTATATCACC	IL22_2-5'	TCCAGCAGCCCTATATCACC
AHR_1-3'	GACGCTGAGCCTAAGAACTGA	AHR_1-3'	GACGCTGAGCCTAAGAACTGA
AHR_2-5'	TAAAGCCAATCCCAGCTGAA	AHR_2-5'	TAAAGCCAATCCCAGCTGAA
CCR4_1-3'	AGCCCACCAAGTACATCCAG	CCR4_1-3'	AGCCCACCAAGTACATCCAG
CCR4_2-5'	CAAATACAAGCGGCTCAGGT	CCR4_2-5'	CAAATACAAGCGGCTCAGGT
GMCSF_1-3'	AGGGCAGTGCTGCTTGTAGT	GMCSF_1-3'	AGGGCAGTGCTGCTTGTAGT
GMCSF_1-5'	CACTGCTGCTGAGATGAATGA	GMCSF_1-5'	CACTGCTGCTGAGATGAATGA

Preamplification		qPCR	
Bcl6_1-3'	AAGTCCAGGAGGATGCAGAA	Bcl6_1-3'	AAGTCCAGGAGGATGCAGAA
Bcl6_2-5'	AGCCGTGAGCAGTTTAGAGC	Bcl6_2-5'	AGCCGTGAGCAGTTTAGAGC
CD4_1-3'	CATTCAGCTTGGATGGACCT	CD4_1-3'	CATTCAGCTTGGATGGACCT
CD4_1-5'	ACCGGGGGAGTCCCTTTTAG	CD4_1-5'	ACCGGGGGAGTCCCTTTTAG
IL2_3-3'	GCACTTCCTCCAGAGTTTG	IL2_3-3'	GCACTTCCTCCAGAGGTTTG
IL2_3-5'	TGGAGCATTTACTGCTGGATT	IL2_3-5'	TGGAGCATTTACTGCTGGATT
CD8_3-5'	GCTGGACTTCGCCTGTGATAT	CD8_3-5'	GCTGGACTTCGCCTGTGATAT
CD8_4-3'	TTGTCTCCCGATTTGACCAC	CD8_4-3'	TTGTCTCCCGATTTGACCAC
CD52_1-3'	CTGAAGCAGAAGAGGTGGATT	CD52_1-3'	CTGAAGCAGAAGAGGTGGATT
CD52_1-5'	GCGCTTCCTCTTCCTCCTAC	CD52_1-5'	GCGCTTCCTCTTCCTCCTAC
RANTES_1-5'	CGCTGTCATCCTCATTGCTA	RANTES_2-5'	ATCTGCCTCCCCATATTCCT
RANTES_1-3'	ACACACTTGGCGGTTCTTTC	RANTES_1-3'	ACACACTTGGCGGTTCTTTC
REL_1-5'	ACAAATGTGAAGGGCGATCA	REL_2-5'	GGAGCACAGCACAGACAACA
REL_1-3'	CCGTCTCTGCAGTCTTTTCC	REL_1-3'	CCGTCTCTGCAGTCTTTTCC
RGS16_2-5'	CACGCTTTCCTGAAGACAGA	RGS16_2-5'	CACGCTTTCCTGAAGACAGA
RGS16_1-3'	GACCTCTTTAGGGGCCTCAC	RGS16_1-3'	GACCTCTTTAGGGGCCTCAC
EOMES_1-3'	GGGACAATCTGATGGGATGA	EOMES_1-3'	GGGACAATCTGATGGGATGA
EOMES_1-5'	CACAAATACCAACCCCGACT	EOMES_1-5'	CACAAATACCAACCCCGACT
CD3e_1-3'	CCTCATCACCGCCTATGTTT	CD3e_1-3'	CCTCATCACCGCCTATGTTT
CD3e_1-5'	GCACTCACTGGAGAGTTCTGG	CD3e_1-5'	GCACTCACTGGAGAGTTCTGG
NFATC2_2-5'	AAGAAGAGCCGAATGCACATA	NFATC2_2-5'	AAGAAGAGCCGAATGCACATA
NFATC2_1-3'	AGAAACTTCTGCGGCCCTAC	NFATC2_1-3'	AGAAACTTCTGCGGCCCTAC
CXCR5_2-5'	AAATGGACCTCGAGAACCTG	CXCR5_2-5'	AAATGGACCTCGAGAACCTG
CXCR5_1-3'	CTTGAAGGAGGCCATGAGG	CXCR5_1-3'	CTTGAAGGAGGCCATGAGG
GZMA_2-5'	GAACAAAAGGTCCCAGGTCA	GZMA_2-5'	GAACAAAAGGTCCCAGGTCA
GZMA_1-3'	TTTTTGCTTTTTCCATCAGC	GZMA_1-3'	TTTTTGCTTTTTCCATCAGC
GZMB_1-5'	GGTGGCTTCCTGATACGAGA	GZMB_2-5'	ACTGTTGGGGAAGCTCCATA
GZMB_1-3'	GCTGCAGTAGCATGATGTCG	GZMB_1-3'	GCTGCAGTAGCATGATGTCG
GZMH_1-5'	CAGCCATTCCTCCTCCTGT	GZMH_2-5'	TCCTCCTGTTGGCCTTTCTT
GZMH_1-3'	GAGCAGCTGTCAGCACAAAG	GZMH_1-3'	GAGCAGCTGTCAGCACAAAG
MIP1B_1-5'	CTGTCCTGTCTCTCCTCATGC	MIP1B_2-5'	TAGCTGCCTTCTGCTCTCCA
MIP1B_1-3'	GCTTGCTTCTTTTGGTTTGG	MIP1B_1-3'	GCTTGCTTCTTTTGGTTTGG
PRF1_1-5'	AACTTTGCAGCCCAGAAGAC	PRF1_2-5'	ACAGCTTCAGCACTGACACG
PRF1_1-3'	GGGTGCCGTAGTTGGAGATA	PRF1_1-3'	GGGTGCCGTAGTTGGAGATA
TNFSF10_1-5'	GACAGACCTGCGTGCTGAT	TNFSF10_2-5'	CCTGCAGTCTCTCTGTGTGG
TNFSF10_1-3'	CAGCAGGGGCTGTTCATACT	TNFSF10_1-3'	CAGCAGGGGCTGTTCATACT
TNFSF6_1-5'	GGGATGTTTCAGCTCTTCCA	TNFSF6_2-5'	CAGAAGGAGCTGGCAGAACT
TNFSF6_1-3'	CAGAGGCATGGACCTTGAGT	TNFSF6_1-3'	CAGAGGCATGGACCTTGAGT
CD27_1-5'	CACTACTGGGCTCAGGGAAA	CD27_2-5'	CTCGTGAAGGACTGTGACCA
CD27_1-3'	GCGAACGAGAAGACCAGAGT	CD27_1-3'	GCGAACGAGAAGACCAGAGT
CD95_1-5'	CAAGGGATTGGAATTGAGGA	CD95_2-5'	ATGGCCAATTCTGCCATAAG
CD95_1-3'	TGGAAGAAAAATGGGCTTTG	CD95_1-3'	TGGAAGAAAAATGGGCTTTG
TGFBR1_1-5'	ACAGATGGGCTCTGCTTTGT	TGFBR1_2-5'	GCACCCTCTTCAAAAACTGG
TGFBR1_1-3'	CAAGGCCAGGTGATGACTTT	TGFBR1_1-3'	CAAGGCCAGGTGATGACTTT
TGFBR2_1-5'	TCCACCTGTGACAACCAGAA	TGFBR2_2-5'	ATGAGCAACTGCAGCATCAC
TGFBR2_1-3'	GGAGAAGCAGCATCTTCCAG	TGFBR2_1-3'	GGAGAAGCAGCATCTTCCAG
FASL_1-5'	GGCCTGTGTCTCCTTGTGAT	FASL_2-5'	GGGATGTTTCAGCTCTTCCA
FASL_1-3'	GTGGCCTATTTGCTTCTCCA	FASL_1-3'	GTGGCCTATTTGCTTCTCCA
Plk_1-5'	CTGCACCGAAACCGAGTTAT	Plk_1-5'	CTGCACCGAAACCGAGTTAT
Plk_1-3'	TCCCACACAGGGTCTTCTTC	Plk_1-3'	TCCCACACAGGGTCTTCTTC
Ube2c_1-5'	TGGCGATAAAGGGATTTCTG	Ube2c_2-5'	TTTCAAATGGGTAGGGACCA
Ube2c_1-3'	GGCGTGAGGAACTTCACTGT	Ube2c_1-3'	GGCGTGAGGAACTTCACTGT
H2afx_1-5'	TACCTCACCGCTGAGATCCT	H2afx_1-5'	TACCTCACCGCTGAGATCCT
H2afx_1-3'	AGCTTGTTGAGCTCCTCGTC	H2afx_2-3'	GTTGAGCTCCTCGTCGTTG
Fos_1-5'	CCGGGGATAGCCTCTCTTAC	Fos_2-5'	ACTACCACTCACCCGCAGAC
Fos_1-3'	ACTGGTCGAGATGGCAGTG	Fos_1-3'	ACTGGTCGAGATGGCAGTG
Aurka_2-5'	GTCACAAGCCGGTTCAGAAT	Aurka_2-5'	GTCACAAGCCGGTTCAGAAT
Aurka_1-3'	TTTGATGCCAGTTCCTCCTC	Aurka_1-3'	TTTGATGCCAGTTCCTCCTC
TMEM2_1-5'	TTGCCCAGATCAAAATCCTC	TMEM2_2-5'	TCTCAGGAATTGGGATCCAG
TMEM2_1-3'	TCCCCAAATACAAGCAGTCC	TMEM2_1-3'	TCCCCAAATACAAGCAGTCC

Table S6. Primers used for gene expression analysis of the individual $ZnT8_{186\text{-}194}$ $MMr^{+}CD8^{+}$ T cells depicted in Fig. S9A.

Members of the ImMaDiab Study Group.

Jean-Claude Carel, Nadia Tubiana-Rufi, Laetitia Martinerie, Amélie Poidvin, Evelyne Jacqz-Aigrain, Laurence Corvez, Véronique Berruer (Robert Debré Hospital, Paris);
Jean-François Gautier, Baz Baz (Saint Louis Hospital, Paris);
Fabrizio Andreelli, Chloé Amouyal, Sophie Jaqueminet, Olivier Bourron, Agnès Hartemann (Pitié-Salpêtrière Hospital, Paris);
Amal Lemoine-Yazigi, Danièle Dubois-Laforgue (Cochin Hospital, Paris);
Florence Travert, Michel Marre (Bichat Hospital, Paris);
Philippe Chanson, Claire Briet (Kremlin-Bicêtre Hospital, Paris);
Pierre-Jean Guillausseau, Leila Ait-Bachir (Lariboisière Hospital, Paris);
Carole Collet, Frédéric Beziaud, Gwenaelle Petit-Aubert (Versailles André Mignot Hospital, Le Chesnay);
Sophie Christin-Maitre, Bruno Fève, Camille Vatier (Saint Antoine Hospital, Paris);
Najiba Lahlou (Laboratory of Hormonology, Cochin Hospital, Paris);
Prissile Bakouboula, Caroline Elie, Hélène Morel, Jean-Marc Treluyer (Clinical Research Unit Paris Centre Descartes, Paris);
Marie-Claude Gagnerault, Claire Maillard, Anna Jones (INSERM U1016, Cochin Institute, Paris).